Supporting Information for

Photochemical production of carbon monoxide from dissolved organic matter: The role of lignin methoxyarene functional groups

Rachele Ossola,* Richard Gruseck, Joanna Houska, Alessandro Manfrin, Morgan Vallieres, and Kristopher McNeill*

E-mail: rachele.ossola@colostate.edu; kristopher.mcneill@env.ethz.ch

48 Pages, 20 Figures, 3 Tables

S1 Chemicals

Acetovanillone (**G2**; 98%), acetosyringone (**S2**; 97%), sodium benzoate (BA; 99%), *p*-hydroxybenzoic acid (99.5%), 1,2-propanediol (99.5%), and methanesulfonic acid (99%) were purchased from Sigma-Aldrich, 4-hydroxyacetophenone (**H2**; > 98%) was from TCI, and methanol (99.9%, HPLC grade) was from Lichrosolv. 4-(1-Hydroxyethyl)-phenol (**H1**), 4-(1-hydroxyethyl)-2-methoxyphenol (**G1**), 4-(1-hydroxyethyl)-2,6-dimethoxyphenol (**S1**), 2-(4-(1-Hydroxyethyl)-2-methoxyphenoxy)propan-1-ol (**GD1**), and 1-(4-hydroxy-3-methoxyphenyl)-2-phenoxypropane-1,3-diol (**GD2**) were synthesized as detailed in Section S1.2. Acetonitrile-d_3 (99 atom% D) and deuterium oxide (99.8 atom% D) were obtained from Armar Isotopes.

For each model compound, we prepared a stock solution ($\approx$ 10 mM) in 20% acetonitrile (ACN; $\geq$ 99.9%, Fisher Chemicals) and 80% nanopure water (18.2 MΩ cm, Barnstead Nanopure Diamond system or Merck Milli-Q IQ 7000 system). The benzoate stock solution ($\approx$ 10 mM) was prepared in 100% nanopure water from its sodium salt, as also small additional amounts of ACN were sufficient to suppress $OH^{\bullet}$ production. Experimental solutions ($\approx$ 50 μM) were obtained upon dilution of the concentrated stocks in nanopure water. For ^{1}H NMR experiments, we dissolved each model compound in acetonitrile-d_3 (0.5% final acetonitrile concentration), and we added D_2O to obtain a $\approx$ 1 mM solution for irradiation.

S2 Synthesis of lignin model compounds

S2.1 Overview of the synthetic procedures

Monomers (H1, G1, S1) α-Alcohol monomers were synthesized upon sodium borohydride ($NaBH_4$) reduction of the corresponding acetyl-protected *p*-hydroxyketones (Figure S1A). Initially, we attempted the reaction on the unprotected substrates (as done by others),[1–4] but reaction yields were unsatisfactory. We therefore hypothesized that $NaBH_4$ was not only acting as a reduging agent, but also as a base. Phenol deprotonation decreased the $NaBH_4$ equivalents available to reduce the ketone and resulted in the formation of stable borate salts, which considerably decreased workup recoveries. We overcame these problems by acetylating the phenol, as in Noij et al.[5] Using this procedure, we obtained total yields of 61% for **H1**, 43% for **G1**, and 11% for **S1**. A direct $NaBH_4$ reduction protocol used in the past in our group gave the same products in 13% (**H1**), 12% (**G1**), and 25% (**S1**) yields.[4] These results suggest that acetylation is effective for **H1** and **G1**, but may not be necessary

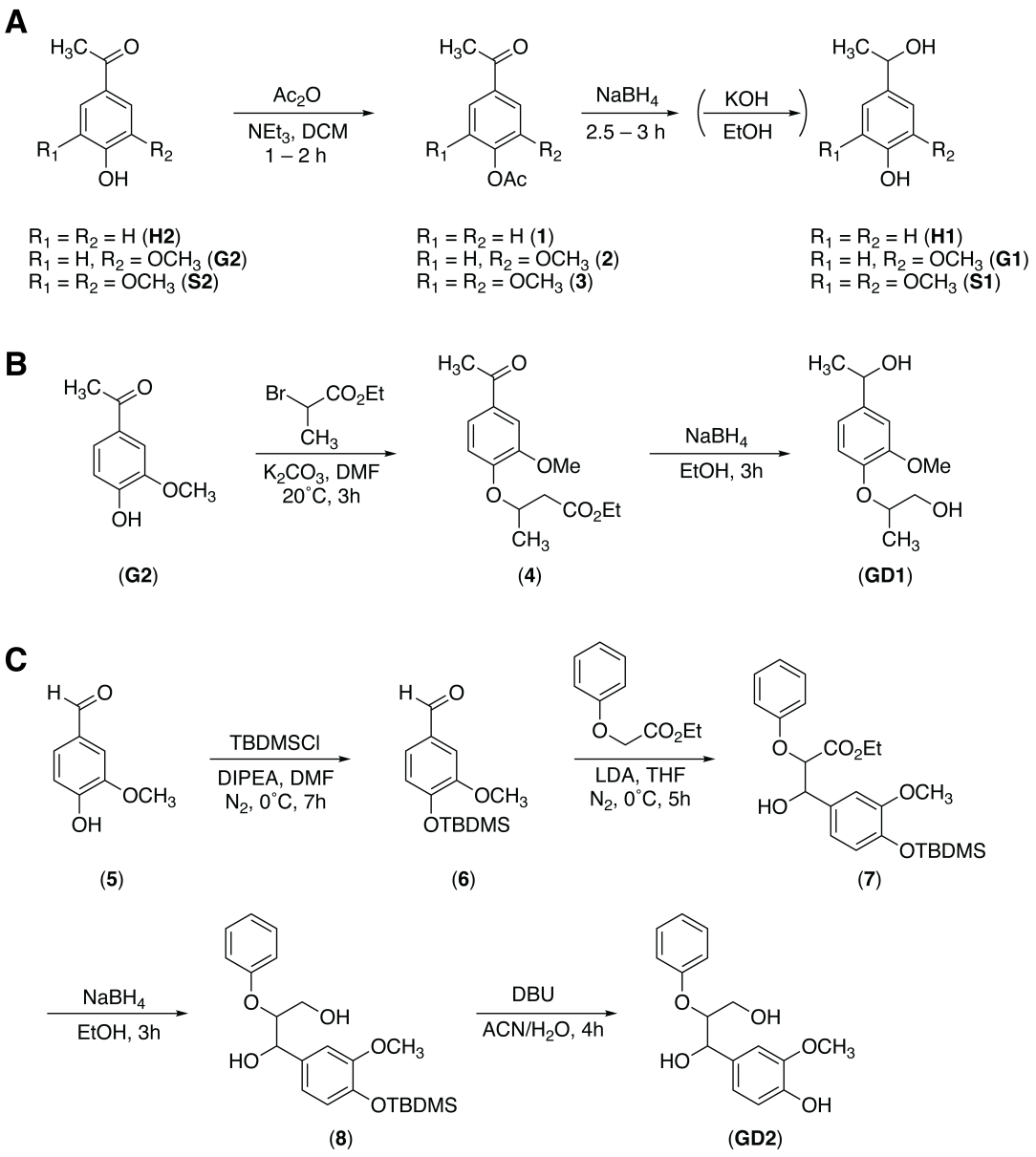

Figure S1: **A** Reaction sequence for the synthesis of **H1**, **G1**, and **S1** from the respective ketones. For **H1**, basic treatment to deprotect the phenol was not performed. **B** Reaction sequence for the synthesis of **GD1** from acetovanillone (**G2**). **C** Reaction sequence for the synthesis of **GD2** from vanillin (**5**). Legend: Ac_2O, acetic anhydride; DBU, 1,8-diazabicyclo(5.4.0)undec-7-ene; DCM, dichloromethane; DIPEA, diisopropylethylamine; DMF, dimethylformamide; EtOH, ethanol; LDA, lithium diisopropylamide; NEt_3, triethylamine.

for **S1**, likely due to differences in steric hindrance.

GD1 The lignin model **GD1** was synthesized in two steps from acetovanillone (**G2**), with an overall yield of 39% (Figure S1B). The synthetic route involves reaction of ethyl-2-bromopropanoate with acetovanillone to yield ethyl 2-(4-acetyl-2-methoxyphenoxy)propanoate (**4**). This intermediate was reduced with sodium borohydride at the ester and ketone functionalities to yield the desired product.

GD2 The lignin dimer **GD2** was obtained in four steps from vanillin (**5**), with an overall yield of 22% (Figure S1C). Vanillin was first protected at the phenolic group with tert-buthyldimethylsilyl chloride (**6**). We then performed an aldol addition between **6** and ethyl 2-phenoxyacetate, resulting in the formation of intermediate **7**. Last, the ethyl ester was reduced with $NaBH_4$ (**8**) and the phenol was deprotected to yield **GD2**. This synthetic route improves the previous scheme developed by McNally et al.,[4] which afforded **GD2** in six step from acetovanillone with an overall yield of 1%.

Our sequence produced a mixture of threo and erythro diastereomers (ratio of 7:3), consistent with previous literature.[4] No attempts were made to separate the two isomers, as previous work found that their photoreactivity is non-stereoselective.[4]

S2.2 Experimental details

Additional chemicals and instruments Triethylamine (NEt_3, $\geq$ 98%), ethyl acetate (AcOEt, $\geq$ 99.7%), sodium borohydride ($NaBH_4$, $\geq$ 96%), *tert*-butyldimehtylsilyl chloride (TBDMSCl, 97%), ethyl 2-phenoxyacetate (98%), lithium diisopropylamide (LDA, 1 M in tetrahydrofuran/ hexane), and ethyl 2-bromopropionate (99%) were purchased from Sigma-Aldrich. Sodium chloride (99.5%), magnesium sulfate (Mg_2SO_4, 62 – 70%), and sodium hydroxide (99.3%) were obtained from Fisher Chemical. Potassium carbonate (K_2CO_3, $\geq$99.0%), *N,N*-dimethylformamide ($\geq$ 99.8%), vanillin ($\geq$ 98%), and ammonium chloride (NH_4Cl, $\geq$ 99%) were purchased from Fluka. Ethanol (EtOH, $\geq$ 99.9%), acetone (100%), dichloromethane (DCM, 100%), and methanol (MeOH, $\geq$ 99.8%) were purchased from VWR. *N,N*-Diisopropylethylamine ($\geq$ 98 %), 4-dimethylaminopyridine (99%), and petroleum ether ($60-95^\circ$ extra pure) were purchased from Acros Organics. Hexane ($\geq$ 98%), tetrahydrofuran (THF, $\geq$ 99.8%), acetic anhydride ($\geq$ 98%), 2-propanol (for analysis), and sodium hydrogen carbonate ($NaHCO_3$) were purchased from Merck. 1,8-Diazabicyclo(5.4.0)undec-7-ene (DBU, 99%) was purchased from Alfa Aesar.

Anhydrous solvents were stored over molecular sieves. Anhydrous THF was purified by distillation with sodium benzophenone. Thin layer chromatography (TLC) was performed on

SiliaPlate glass-backed TLC extra hard layer 60Å (Silicycle Inc.). For flash chromatography, we used SiliaFlash P60 silica gel 40 – 63μ (230–400 mesh, Silicycle Inc.). Preparative HPLC was performed using an amide column (SUPELCO Analytical Ascentis RP-AMIDE 10 cm × 21.2 mm, 5 μm). ^{1}H NMR and ^{13}C NMR spectral data were recorded on a Bruker AVANCE *III* 400 spectrometer at 400 and 100 MHz, respectively. The chemical shifts were referenced to the corresponding residual solvent signal ($CDCl_3$: δH = 7.26 ppm, δC = 77.16 ppm; MeOD: δH = 3.31 ppm, δC = 49.00 ppm).[6]

4-Acetylphenyl acetate (1) Acetic anhydride (Ac_2O; 0.21 mL, 2.2 mmol) was slowly added to a solution of *p*-hydroxyacetophenone (**H2**; 273 mg, 2.0 mmol) and triethylamine (NEt_3; 0.56 mL, 4.0 mmol) in DCM (4 mL). The mixture was stirred for 1 h until completion (monitored via TLC, AcOEt:hexane 1:1), then acidic H_2O (5 mL) was added, and the mixture was extracted with DCM (2 × 5 mL). The combined organic fractions were washed with a HCl solution (1 M, 5 mL) and with brine (10 mL). They were then dried over Mg_2SO_4, filtered, and concentrated under reduced pressure to give the desired product in quantitative yields (colourless liquid, > 360 mg, 100%). ^{1}H NMR (400 MHz, MeOD) $\delta = 8.06 - 7.98$ (m, 2H), $7.26 - 7.19$ (m, 2H), 2.59 (s, 3H), 2.30 (s, 3H). This procedure was adapted from Noji et al.[5]

4-(1-Hydroxyethyl)-phenol (H1) The crude product **1** (> 360 mg, 2.0 mmol) was dissolved in EtOH (10 mL) at 0°C, then $NaBH_4$ (171 mg, 4.5 mmol) was added portionwise under gentle stirring. The mixture was allowed to warm to room temperature and was left to react for 3 h. The reaction was followed via TLC (AcOEt:hexane 1:1). At completion, the excess of $NaBH_4$ was quenched with acetone (3 mL) and the mixture was concentrated at reduced pressure to yield a white solid. The solid was redissolved in H_2O (25 mL) and was extracted with AcOEt (3 × 25 mL). The combined organic phases were washed with brine (15 mL), anhydrified over Mg_2SO_4, filtered, and the solvent was removed at reduced pressure to yield **H1** as a white solid (168 mg, 1.22 mmol, 61%). ^{1}H NMR and ^{13}C NMR confirmed that the reaction yielded directly the deprotected phenol. The compound was recrystallized from toluene. ^{1}H NMR (400 MHz, MeOD) $\delta = 7.21 - 7.14$ (m, 2H), $6.77 - 6.70$ (m, 2H), 4.73 (q, J = 6.5 Hz, 1H), 1.40 (d, J = 6.5 Hz, 3H). ^{13}C NMR (100 MHz, MeOD) δ = 157.6, 138.4, 127.8, 115.9, 70.6, 25.4. This procedure was adapted from Noji et al.[5]

4-Acetyl-2-methoxyphenyl acetate (2) Acetic anhydride (Ac_2O; 0.55 mL, 5.5 mmol) was slowly added to a solution of acetovanillone (**G2**; 830 mg, 5.0 mmol) and triethylamine

(NEt_3; 1.4 mL, 10 mmol) in DCM (7.5 mL). The mixture was stirred for 2 h, then acidic H_2O (10 mL) was added and the reaction mixture was extracted with DCM (2 × 10 mL). The combined organic fractions were washed with brine (10 mL), saturated NH_4Cl (10 mL), and were then dried over Mg_2SO_4, filtered, and concentrated under reduced pressure to give the desired product in quantitative yields (≈ 1.3 g, 100%). ^{1}H NMR (400 MHz, MeOD) δ = 7.63 (m, 1H), 7.16 (dd, J = 8.7, 1.1 Hz, 2H), 3.88 (s, 3H), 2.60 (s, 3H), 2.28 (s, 3H). This procedure was adapted from Noji et al.[5]

4-(1-Hydroxyethyl)-2-methoxyphenol (G1) $NaBH_4$ (178 mg, 4.70 mmol) was added portionwise to a solution of **2** (969 mg, 4.65 mmol) in 2-propanol (10 mL) kept at 0°C. The mixture was stirred for 2.5 h while allowed to warm to room temperature. Excess of $NaBH_4$ was decomposed by addition of acetone (1 mL). The mixture was concentrated under reduced pressure and the residue was partitioned between AcOEt and H_2O. The aqueous layer was extracted with AcOEt (3 × 15 mL). The combined organic fractions were washed with brine (20 mL), dried over Mg_2SO_4, filtered, and concentrated under reduced pressure. The residue was dissolved in EtOH (5 mL) and a aqueous KOH solution was added (1.5 mL of a 4 M solution, 6 mmol). The mixture was stirred overnight at room temperature and then concentrated under reduced pressure. The residue was partitioned between AcOEt and saturated aqueous NH_4Cl, and the aqueous layer was extracted with AcOEt (3 × 15 mL). The combined organic fractions were washed with brine (20 mL), dried over Mg_2SO_4, and concentrated under reduced pressure. The crude product was recrystallized from petroleum ether/DCM to give the desire product as a white solid (333 mg, 43%). ^{1}H NMR (400 MHz, $CDCl_3$) δ = 6.94 (d, J = 1.8 Hz, 1H), 6.91 – 6.81 (m, 2H), 5.58 (s, 1H), 4.84 (m, 1H), 3.91 (s, 3H), 1.75 (d, J = 2.8 Hz, 1H), 1.48 (d, J = 6.4 Hz, 3H). ^{13}C NMR (100 MHz, $CDCl_3$) δ = 146.8, 145.2, 138.1, 118.5, 114.3, 108.1, 70.5, 56.1, 25.3. This procedure was adapted from Noji et al.[5]

4-Acetyl-2,6-dimethoxyphenyl acetate (3) Acetic anhydride (Ac_2O; 0.72 mL, 7.65 mmol) was slowly added to a solution of acetosyringone (**S2**; 1 g, 5.1 mmol), triethylamine (NEt_3; 1.06 mL, 7.65 mmol), and 4-dimethylaminopyridine (DMAP; 13 mg, 0.1 mmol) in DCM (30 mL) kept at 0°C. The mixture was stirred for 1.5 h while allowed to warm to room temperature. H_2O (20 mL) was then added to the mixture and the organic phase was extracted with DCM (3 × 20 mL). The combined organic fractions were washed with saturated aqueous NH_4Cl (20 mL) and brine (20 mL), and then dried over Mg_2SO_4, filtered, and concentrated under reduced pressure to give the desired product in quantitative yields

(1.22 g, 100%). ^{1}H NMR (400 MHz, $CDCl_3$) δ = 7.23 (s, 2H), 3.89 (s, 6H), 2.60 (s, 3H), 2.36 (s, 3H). ^{13}C NMR (100 MHz, $CDCl_3$) δ = 196.9, 168.3, 152.4, 135.3, 133.0, 105.3, 56.5, 26.7, 20.6. This procedure was adapted from Noji et al.[5]

4-(1-Hydroxyethyl)-2,6-dimethoxyphenol (S1) $NaBH_4$ (195 mg, 5.15 mmol) was added portionwise to a solution of **3** (1.22 g, 4.65 mmol) in 2-propanol/DCM (10 mL + 5 mL) kept at 0°C. The mixture was stirred for 2.5 h while allowed to warm to room temperature. Excess of $NaBH_4$ was decomposed by addition of acetone (1 mL). The mixture was concentrated under reduced pressure and the residue was partitioned between AcOEt and H_2O. The aqueous layer was extracted with AcOEt (3 × 20 mL) and the combined organic fractions were washed with brine (20 mL), dried over Mg_2SO_4, filtered, and concentrated under reduced pressure. The residue was dissolved in EtOH (10 mL) and an aqueous KOH solution was added (1 mL of a 4 M solution, 4 mmol). The mixture was stirred overnight at room temperature and then concentrated under reduced pressure. The residue was partitioned between AcOEt and saturated aqueous NH_4Cl, then the aqueous layer was extracted with AcOEt (3 × 20 mL). The combined organic fractions were washed with brine (20 mL), dried over Mg_2SO_4, and concentrated under reduced pressure. The crude product was purified by flash chromatography (4:1 DCM:AcOEt) to give the desired compound as a light orange solid (100 mg, 11%). ^{1}H NMR (400 MHz, $CDCl_3$) δ = 6.62 (s, 2H), 4.83 (q, J = 6.4 Hz, 1H), 3.91 (s, 6H), 1.49 (d, J = 6.4 Hz, 3H). ^{13}C NMR (100 MHz, $CDCl_3$) δ = 147.2, 137.31, 134.2, 102.2, 70.8, 56.4, 25.4. This procedure was adapted from Noji et al.[5]

Ethyl 2-(4-acetyl-2-methoxyphenoxy)propanoate (4) A solution of acetovanillone (**G2**; 502.3 mg, 3 mmol), ethyl 2-bromopropionate (390 μL, 3 mmol), and K_2CO_3 (621.6 mg, 4.5 mmol) in DMF (10 mL) was stirred at 80°C with a condenser for 3 h. DMF was removed at reduced pressure and the residue was partitioned between water (15 mL) and AcOEt (15 mL). The organic fraction was washed with brine, dried over Mg_2SO_4, filtered, and concentrated under vacuum to give **4** as a mixture of a white and orange solid (797.6 mg, 100%). ^{1}H NMR (400 MHz, $CDCl_3$) δ = 7.55 (d, J = 2.0 Hz, 1H), 7.50 (dd, J = 8.3, 2.0 Hz, 1H), 6.80 (d, J = 8.3 Hz, 1H), 4.85 (q, J = 6.8 Hz, 1H), 4.22 (qd, J = 7.1, 1.5 Hz, 2H), 3.93 (s, 3H), 2.56 (s, 3H), 1.70 (d, J = 6.8 Hz, 3H), 1.25 (t, J = 7.1 Hz, 3H). ^{13}C NMR (100 MHz, $CDCl_3$) δ = 196.9, 171.7, 151.5, 149.8, 131.7, 122.9, 113.6, 111.3, 73.8, 61.6, 56.3, 26.4, 18.6, 14.3. The procedure was adapted from Wimmer et al.[7] and Glock et al.[8]

2-(4-(1-Hydroxyethyl)-2-methoxyphenoxy)propan-1-ol (GD1) $NaBH_4$ (568.5 mg, 15 mmol) was added portionwise to a stirred solution of **4** (398.2 mg, 1.50 mmol) in dry EtOH (6 mL) at 50°C. After 2 h of stirring with a condenser, the reaction was quenched with acetone, resulting in the formation of gas and a white precipitate. The solvents were removed under vacuum and the residue was partitioned between water (10 mL) and AcOEt (15 mL). The organic fraction was washed with brine, dried over Mg_2SO_4, filtered, and concentrated under vacuum, resulting in 282.4 mg of a mixture of **GD1** and **4**. The mixture was reduced again following the same procedure ($NaBH_4$: 114.57 mg, 3 mmol) and was stirred until all of the starting material was reduced (as confirmed by ^{1}H NMR analysis). Purification of the residue by flash chromatography (1:15 MeOH:DCM) gave **5** as a colourless liquid (142.3 mg, 42%). The crude product was further purified by prep-HPLC (75:25 H_2O:ACN), yielding 133.3 mg (0.59 mol, 39%) of **GD1** as a colorless oil. The product was a racemic mixture of two diastereomers. ^{1}H NMR (400 MHz, $CDCl_3$): δ **A** and **B** = 6.99 – 6.92 (m, 2H), 6.87 (dd, J = 8.2, 2.0 Hz, 1H), 4.86 (qd, J = 6.4, 2.8 Hz, 1H), 4.33 – 4.20 (m, 1H), 3.86 (d, J = 4.6 Hz, 3H), 3.70 – 3.61 (m, 2H), 2.92 (dt, J = 9.6, 6.7 Hz, 1H), 1.91 (dd, J = 10.9, 3.4 Hz, 1H), 1.49 (dd, J = 6.4, 0.8 Hz, 3H), 1.33 (dd, J = 6.3, 1.2 Hz, 3H). ^{13}C NMR (100 MHz, $CDCl_3$): δ **A** and **B** = 151.10, 151.07, 146.5, 140.93, 140.91, 119.04, 118.95, 117.93, 109.32, 109.29, 79.33, 79.27, 70.20, 66.06, 55.84, 55.82, 25.15, 16.65, 16.62. This procedure was adapted from Lancefield and Westwood.[9]

4-((t-Butyldimethylsilyl)oxy)-3-methoxybenzaldehyde (6) A solution of vanillin (**5**; 1.26 g, 8.3 mmol) in dry DMF (10 mL) was cooled to 0°C under inert atmosphere. Diisopropylethylamine (DIPEA; 2.9 mL, 16.6 mmol) was added and the mixture was stirred for 10 min. A 1 M solution of *t*-butyldimethylsilyl chloride (TBDMSCl) in THF (10 mL, 10 mmol) was then added dropwise over 20 min. The reaction was followed via TLC (2:1 AcOEt:hexane) until completion. After 7 h, a 0.1 M NaOH (50 mL) solution was added to the mixture, and the resulting was extracted with DCM (2 × 25 mL). The combined organic fractions were washed with saturated aqueous $NaHCO_3$ (30 mL) and water (30 mL), dried over Mg_2SO_4, filtered, and concentrated under reduced pressure to give **6** as a yellow oil (2.26 g, 8.48 mmol, 102%). ^{1}H NMR (400 MHz, $CDCl_3$) δ = 9.85 (s, 1H), 7.40 (d, J = 1.9 Hz, 1H), 7.37 (dd, J = 8.0, 1.9 Hz, 1H), 6.96 (d, J = 8.0 Hz, 1H), 3.87 (s, 3H), 1.00 (s, 9H), 0.19 (s, 6H). ^{13}C NMR (100 MHz, $CDCl_3$) δ = 191.2, 151.8, 151.5, 131.1, 126.4, 120.9, 110.3, 55.6, 25.8, 18.7, −4.4. This procedure was adapted from Reddy et al.[10]

Ethyl 3-(4-((tert-butyldimethylsilyl)oxy)-3-methoxyphenyl)-3-hydroxy-2-phenoxypropanoate (7) A solution of lithium diisopropylamide (LDA; 1 M in THF, 9 mL, 9 mmol) was added dropwise to a stirred solution of **6** (2.26 mg, 8.3 mmol) and ethyl 2-phenoxyacetate (1.36 mL, 8.3 mmol) in distilled THF (100 mL) kept at 0°C under N_2. The reaction progress was followed by ^{1}H NMR. After 6 h, a saturated NH_4Cl solution (50 mL) was carefully added to the reaction mixture, resulting in the formation of a white precipitate. The mixture was partitioned between water (50 mL) and AcOEt (100 mL). The organic fraction was washed with brine (100 mL), dried over Mg_2SO_4, filtered, and concentrated under vacuum. The resulting material was purified via flash chromatography (2:1 hexane:AcOEt). A second flash chromatography was performed to remove excess of phenoxyacetate (4:1 DCM:hexane). After 300 mL of eluent, the column was flushed with methanol to give **7** as a yellow liquid (2.231 g, 60.2%). The product was a racemic mixture (1:1) of the two diastereomers. ^{1}H NMR (400 MHz, $CDCl_3$) δ **A** and **B** = 7.30 – 7.19 (m, 1H), 7.03 – 6.78 (m, 6H), 5.14 (t, J = 5.1 Hz, 0.5H), 5.09 (t, J = 5.1 Hz, 0.5H), 4.72 (d, J = 6.1 Hz, 0.5H), 4.68 (d, J = 5.9 Hz, 0.5H), 4.24 – 4.00 (m, 2H), 3.80 (s, 1H), 3.79 (s, 1H), 2.93 (d, J = 4.3 Hz, 0.5H), 2.82 (d, J = 4.1 Hz, 0.5H), 1.16 (t, J = 7.1 Hz, 1.5H), 1.10 (t, J = 7.1 Hz, 1.5H), 0.99 (s, 9H), 0.14 (s, 6H). ^{13}C NMR (100 MHz, $CDCl_3$) δ **A** and **B** = 169.92, 169.56, 157.76, 157.74, 151.22, 151.06, 145.48, 145.25, 132.73, 131.86, 129.78, 129.69, 122.44, 122.29, 120.89, 120.85, 119.57, 119.38, 115.78, 115.75, 110.89, 110.78, 82.17, 81.14, 74.95, 74.29, 61.59, 55.67, 25.86, 18.61, 14.21, 14.14, −4.50. This procedure was adapted from Lancefield and Westwood.[9]

1-(4-((tert-Butyldimethylsilyl)oxy)-3-methoxyphenyl)-2-phenoxypropane -1,3-diol (8) $NaBH_4$ (317.8 mg, 8.4 mmol) was added portionwise to a stirred solution of **7** (≈ 0.5 g, ≈ 1.12 mmol) in dry EtOH (7 mL) kept at 50°C. After 3 h, the reaction was quenched with acetone (4 mL). The solvents were removed at reduced pressure to yield white crystals and a yellow liquid. The mixture was partitioned between water (20 mL) and AcOEt (20 mL), and the aqueous phase was extracted with AcOEt (20 mL). The combined organic fractions were washed with brine (30 mL), dried over Mg_2SO_4, filtered, and concentrated under vacuum to give **8** as a yellow oil (410 mg, ≈ 90%). The product was a mixture of two diastereomers (7:3). The major compound is labeled **A**, the minor **B**. ^{1}H NMR (400 MHz, $CDCl_3$) $\delta_{\mathbf{A}}$ = 7.32 – 7.20 (m, 2H), 7.03 – 6.79 (m, 6H), 5.03 (dd, J = 5.5, 3.2 Hz, 1H), 4.40 (p, J = 4.9 Hz, 1H), 4.00 – 3.85 (m, 2H), 3.78 (s, 3H), 2.59 (d, J = 3.3 Hz, 1H), 2.10 (t, J = 6.5 Hz, 1H), 0.98 (s, 9H), 0.13 (s, 6H). $\delta_{\mathbf{B}}$ = 7.32 – 7.20 (m, 2H), 7.03 – 6.79 (m, 6H), 4.97

(dd, J = 6.8, 2.9 Hz, 1H), 4.40 (p, J = 4.9 Hz, 1H), 4.00 – 3.85 (m, 1H), 3.80 (s, 3H), 3.59 (ddd, J = 11.9, 7.7, 4.0 Hz, 1H), 2.74 (d, J = 3.0 Hz, 1H), 1.67 (dd, J = 7.5, 5.2 Hz, 1H), 0.99 (s, 9H), 0.14 (s, 6H). ^{13}C NMR (100 MHz, $CDCl_3$): $\delta_{\mathbf{A}}$ = 157.9, 151.3, 145.0, 133.9, 129.8, 122.1, 121.2, 118.8, 116.78, 110.4, 82.3, 74.2, 61.7, 55.7, 25.9, 18.6, −4.5. $\delta_{\mathbf{B}}$ = 157.9, 151.3, 145.0, 133.2, 129.9, 122.2, 121.1, 119.5, 116.7, 110.8, 83.5, 74.2, 61.5, 55.7, 25.9, 18.6, −4.5. This procedure was adapted from Lancefield and Westwood.[9]

1-(4-Hydroxy-3-methoxyphenyl)-2-phenoxypropane-1,3-diol (GD2) DBU (37 μL, 0.25 mmol) was added to a stirred solution of **8** (98.5 mg, 10.24 mmol) in ACN and H_2O (95:5, 25 mL). The reaction progress was monitored via TLC (3:1 AcOEt:petrolum ether). After 4.5 h, a saturated NH_4Cl solution (1 mL) was added and the mixture was extracted with DCM (2 × 5 mL). The combined organic fractions were dried over Mg_2SO_4, filtered, and concentrated under vacuum. The mixture was diluted in DCM, loaded on silica, and purified with flash chromatography (4:1 AcOEt:hexane). The crude product was further purified by prep-HPLC (60:40 H_2O:ACN) to obtain **GD2** as a colorless liquid (27 mg, 39%). The product was a mixture of two diastereomers (7:3). The major compound is labeled **A**, the minor **B**. ^{1}H NMR (400 MHz, $CDCl_3$) $\delta_{\mathbf{A}}$ = 7.33 – 7.21 (m, 2H), 7.04 – 6.85 (m, 6H), 5.58 (s, 1H), 5.03 (dd, J = 5.4, 3.0 Hz, 1H), 4.45 – 4.35 (m, 1H), 4.00 – 3.89 (m, 2H), 3.87 (s, 3H), 2.64 (d, J = 3.3 Hz, 1H), 2.13 (t, J = 6.4 Hz, 1H). $\delta_{\mathbf{B}}$ = 7.33 – 7.21 (m, 2H), 7.04 – 6.85 (m, 6H), 5.62 (s, 1H), 4.98 (dd, J = 6.9, 2.7 Hz, 1H), 4.45 – 4.35 (m, 1H), 4.00 – 3.89 (m, 1H), 3.89 (s, 3H), 3.60 (ddd, J = 11.8, 7.3, 4.0 Hz, 1H), 2.76 (d, J = 2.9 Hz, 1H), 1.72 (dd, J = 7.5, 5.3 Hz, 1H). ^{13}C NMR (100 MHz, $CDCl_3$) $\delta_{\mathbf{A}}$ = 157.8, 146.8, 145.5, 132.4, 129.8, 122.1, 119.5, 116.7, 114.5, 109.0, 82.1, 74.2, 61.6, 56.1. $\delta_{\mathbf{B}}$ = 158.2, 146.9, 145.9, 131.7, 129.9, 122.2, 120.2, 116.7, 114.5, 109.5, 83.4, 74.2, 61.4, 56.1. This procedure was adapted from Yeom et al.[11]

S3 Speciation of lignin model compouds

α-Alcohols α-Alcohols behave as common phenols, with pK_a values in the range $9.9-10.1$. Specifically, **H1** and **G1** have both pK_a of 9.9,[4] **S1** of 10.1,[4] and **GD2** of 10.0.[4] The pK_a value of **GD1** has not be reported in the literature, but it is expected to lay in this range based on structural similarities with other α-alcohols. Given these dissociation constants, all α-alcohols are expected to be fully protonated at the experimental pH.

α-Ketones α-Ketones have pK_a values between 7.7 and 7.9. Specifically, we obtained dissociation constants of 7.93 for **H2**, 7.77 for **G2**, and 7.77 for **S2** via UV-vis spectroscopy using a method analogous to Martinez and Dardonville.[12] These values agree with previously reported pK_a of $7.75 - 8.05$ for **H2**[13–15] and of $7.4 - 7.5$ for **G2**.[16,17] Using our measured values, we calculated that $0.7 - 1.8\%$ of **H2** and $1.1 - 2.6\%$ of **G2** and **S2** are deprotonated at the experimental pH ($5.8 - 6.2$). We validated this calculation by confirming that the UV-vis spectrum of the three compounds in nanopure water is analogous to the one collected in a pH 6 buffer.

S4 Additional details CO experiments

S4.1 Preparation of the headspace-free test tubes for irradiation

We aliquoted each experimental solution (50 μM) into fourteen borosilicate test tubes (six time points + time zero, in duplicate). The test tubes were filled until the very top ($\approx$ 10 mL) and sealed with a white rubber septum (Sigma Aldrich Precision Seal). Before each use, rubber septa were rinsed three times with deionized water and air dried. Only septa that did not show signs of photochemical damage (e.g., yellowing) were used. A short disposable needle was inserted into the rubber stopper to aid removal of the air trapped between the interior of the septum and the liquid surface. The needle was immediately removed when the septum was correctly inserted onto the test tube head. Each test tube was then carefully inspected to ensure minimal presence of residual air bubbles. In the presence of bubbles larger than $\approx$ 1 mm in dimeter, the test tube was discarded and a new one was prepared.

S4.2 Preparation of vials for headspace GC analyses

Serum vials preparation We first placed 100 μL of HCl 1 M into clean 20 mL serum vials.[1] Each vial was then capped with a butyl septum, crimped, flushed with N_2 for 30 s to obtain a final overpressure of 0.5 bar, and weighted on a scale.

Liquid addition to serum vials Irradiated headspace-free test tubes were first allowed to equilibrate to room temperature. We then used a 10 mL gas-tight plastic syringe (Omnifix Luer Lock Solo, Braun) equipped with a 3-way valve (Discofix C, Braun) and a long needle (Sterican, Braun, 0.80 $\times$ 120 mm, 21 G $\times$ 4 ¾") to withdraw liquid from the headspace-free test tubes. The syringe was first flushed with N_2, then the needle was inserted until the very bottom of the test tube. While starting to withdraw the liquid, a second, short needle (Sterican, Braun, 0.60 $\times$ 25 mm, 23 G $\times$ 1") was inserted into the test tube septum to avoid creating negative pressure. The syringe was gently filled until $\approx$ 6.5 mL, then the 3-way valve was closed, the long needle was carefully replaced with a short needle (Sterican, Braun, 0.60 $\times$ 25 mm, 23 G $\times$ 1") while keeping the syringe vertical, and $\approx$ 6 mL of liquid were rapidly injected into a nitrogen-flushed 20 mL serum vial. At the end of the injection, the 3-way valve was closed and the needle was carefully removed from the butyl septum.

[1] Note that samples acidification is not needed for CO analyses. This step is a legacy of a protocol for quantification of both CO and CO_2 (see Borduas-Dedekind et al.[18]).

The serum vials were later weighted for accurate quantification of the liquid volume and were stored at 4°C until analyses (always performed within a week of preparation).

S5 Optimization of experimental conditions for ^{1}H NMR

Glassware and experimental protocol Due to high detection limits of this analytical technique, we performed ^{1}H NMR experiments using 20-fold more concentrated solutions compared to other experiments described in this work (i.e., 1 mM instead of 50 μM). These concentrations allow one obtaining neat ^{1}H NMR spectra but they also introduce screening limitations that considerably lower photochemical rates. We calculated that $< 10\%$ of the incoming photons (at 313 nm) are absorbed within 1 mm from the surface in a 50 μM solution of **G2**, while this number increases to $> 80\%$ at 1 mM.

We confirmed these observations by irradiating the same 1 mM solution of **G2** in D_2O in a borosilocate test tube (inner diameter = 13.4 mm) and in an NMR tube (inner diameter = 2.5 mm). The NMR tube was either shaked periodically (each 30 min) or was left untouched for the whole experiment. Figure S2A shows that pseudo-first-order decay occurs only if the solution is irradiated in a NMR tube and is mixed periodically (filled circles, $k_{obs} = (0.328 \pm 0.017)$ h^{-1}). In the absence of mixing, photodegradation stops after 30 min of irradiation in an NMR tube (filled squares), and is almost completely inhibited in a borosilicate test tube (open triangles) – in agreement with differences in test tubes' inner diameter. This result also proves that NMR tubes have comparable (if not higher) UVB transparency to borosilicate tubes and can reliably be used in our irradiation setup.

We further consolidated these findings by irradiating (6 lamps) increasing concentrations of **G2** (50 μM to 1 mM in nanopure water) in borosilicate test tubes. The solutions were not mixed during the irradiation. The dramatic decrease in **G2** photodegradation as a function of the initial substrate concentration (Figure S2B) agrees with results obtained in D_2O using NMR tubes. Indeed, the pseudo-first-order rate constant at 1 mM ($k_{obs} = (0.086 \pm 0.009)$ h^{-1}) was only 5% of its value at 50 μM ($k_{obs} = (1.69 \pm 0.05)$ h^{-1}) and was comparable to the value in the 1 mM D_2O solution ($k_{obs} = (0.025 \pm 0.023)$ h^{-1}; empty triangles in Figure S2A).

Internal standard As the internal standard, we selected methanesulfonic acid (CH_3SO_3H, MSA) due to its convenient spectroscopic and photochemical features. Its ^{1}H NMR spectrum features a singlet at $\delta = 2.81$ ppm, which does not overlap with any of the substrates or products peaks. At the solution pH, MSA is present as a fully deprotonated sulfonate ($pK_a < 1$) and its presence does not affect the solution pH. Furthermore, MSA is photochemically stable (see Ossola et al.[19] and Text S6.2) and does not influence the parent compound degradation kinetics nor the methanol production kinetics (Text S6.2).

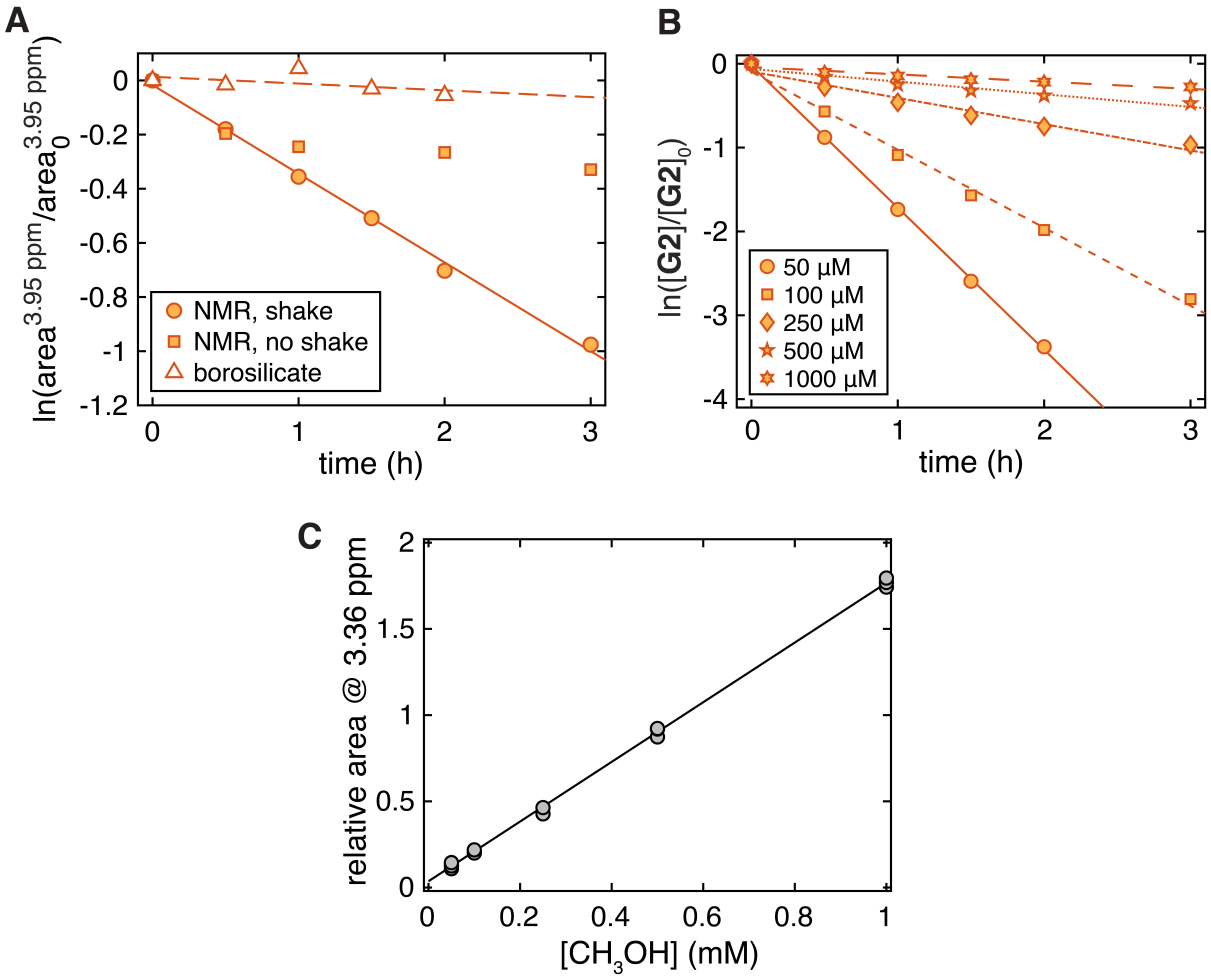

Figure S2: **A** Changes in **G2** photodegradation kinetics for different experimental conditions ($\approx$ 1 mM in D_2O + 0.5% ACN-d_3, 6 UV lamps). We performed the kinetic analysis using the relative area of the peak at $\delta = 3.95$ ppm, which corresponds to the three protons of the methoxy aromatic group of **G2** (Ar-OC**H$_3$**). **B** Changes in **G2** photodegradation kinetics as a function of initial substrate concentration (6 UV lamps). Solutions were prepared in nanopure water; the irradiation was performed in borosilicate test tubes and **G2** concentrations were determined via HPLC. Each point is the average of a duplicate experiments and lines are linear regressions. Error bars are not reported. **C** Methanol calibration plot. Each point is a single measurement, and the line a linear regression (details in text).

Methanol calibration Methanol was quantified from the relative areas of the singlet at $\delta = 3.36$ ppm using the calibration line in Figure S2C. Areas are relative to the internal standard, which was always present at a concentration of 0.475 mM. Calibration solutions were prepared in D_2O using a 0.1% (v/v) CH_3OH stock solution in D_2O obtained upon dilution of pure methanol and were measured several times across different days. By combining

all data, we obtained the following calibration equation: $y = (1.73 \pm 0.04)x + (0.015 \pm 0.007)$ ($N = 16$, $R^2 = 0.999$). From replicate measurements of the lowest concentration standard (0.05 mM, $N = 5$), we calculated a detection limit of 0.026 mM.

Matrix effects We performed additional measurements to confirm that the calibration line obtained in pure D_2O could be used also in the presence of other solution components - thus, that matrix effects are negligible. First, at the end of each ^1H NMR experiment, we spiked $\approx$ 0.18 mM of CH_3OH and quantified the enhancement in the relative area of the methanol peak. Overall, we measured an average enhancement of 0.329 ± 0.020 (relative error of $\pm 6.1\%$), which corresponds to a concentration of (0.17 ± 0.01) mM. Second, we evaluated changes in the absolute area of the internal standard across all ^1H NMR spectra acquired. For spectra collected in D_2O (+ 0.5% ACN-d_3), the average absolute area was $(3.43 \pm 0.22) \times 10^3$ ($N = 72$), thus the relative error was $\pm 6.4\%$ across all measurements. As a comparison, the absolute area of the internal standard changed to $(3.34 \pm 0.15) \times 10^2$ in the presence of 12.5% H_2O ($N = 7, -90\%$) and to $(1.66 \pm 0.19) \times 10^3$ in the presence of 2.5% ACN ($N = 3, -51\%$). The excellent agreement between theoretical and measured CH_3OH addition, and the minor variations in the absolute area of the internal standard confirms that matrix effects, if present, are minimal.

S6 Control experiments

S6.1 Carbon monoxide

Dark control A solution containing **G2** in nanopure water (50 μM) was irradiated in headspace-free test tubes covered with Al foil. After 6 h of UV irradiation (6 lamps), we measured $[CO]_{6h} = -(0.007 \pm 0.024)$ μM ($N = 4$). As a comparison, the same solution exposed to light produced $[CO]_{6h} = (12.0 \pm 1.0)$ μM ($N = 3$), confirming that CO cannot be generated in the absence of UV irradiation.

Cosolvent control Solutions containing **G2** or **H2** in nanopure water (50 μM) were amended with 1% of acetonitrile (ACN) and irradiated in headspace-free test tubes (6 UV lamps). The added amount is 10-fold higher than in unamended experimental solutions, which contain 0.1% ACN to aid solubilize the model compounds. After 6 hour of irradiation, we measured $[CO]_{6h} = (12.0 \pm 1.0)$ μM ($N = 3$, unamended) and (12.55 ± 0.06) μM ($N = 2$, amended) for **G2**, while for **H2** we obtained $[CO]_{6h} = (2.36 \pm 0.35)$ μM ($N = 2$, unamended) and (2.41 ± 0.14) μM ($N = 2$, amended). Likewise, we did not observe changes in CO photoproduction (Figure S3) nor parent compound degradation kinetics between amended and unamended solutions. These results strongly suggest that ACN concentrations between 0.1 and 1% (v/v) have no effect on CO production.

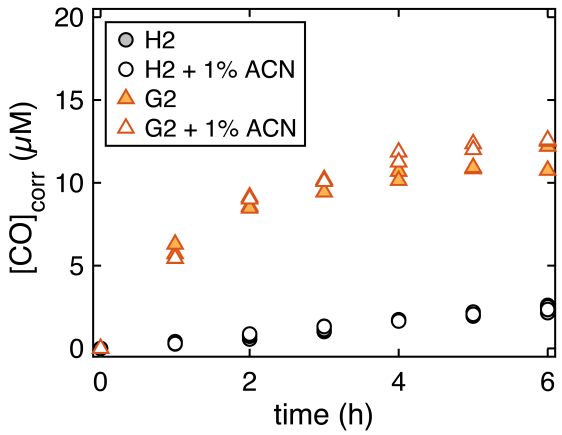

Figure S3: CO photoproduction kinetics of **G2** and **H2** in the presence of 1% ACN (open symbols) as compared to the unamended samples (filled symbols). Each symbol is an individual measurement.

S6.2 Methanol

Dark control We irradiated a solution containing **G2** ($\approx$ 1 mM) in D_2O into an NMR tube wrapped with Al foil (4 h, 6 UV lamps). Every 30 min, we shaked the test tube vigorously to mix the solution. At 0 and 4 h of irradiation, we collected a ^{1}H NMR spectrum and an aliquot for UPLC quantification of **G2**. ^{1}H NMR spectra before and after irradiation did not show any peak at $\delta = 3.36$ ppm. We also calculated $[\mathbf{G2}]/[\mathbf{G2}]_0 = 0.98$ from the UPLC data and 0.96 from the area of the methoxy aromatic protons (singlet, $\delta = 3.95$ ppm). When the test tube was not wrapped in Al foil, $[\mathbf{G2}]/[\mathbf{G2}]_0 = 0.17$ and $[CH_3OH] = 0.22$ mM after 4 h of UV irradiation ($[\mathbf{G2}]_0 = 1.09$ mM). These results confirmed that **G2** is stable in the absence of irradiation, and that methanol is produced only during photodegradation of lignin model compounds.

MSA stability and influence on the reaction kinetics To confirm the photochemical stability of the internal standard, we extracted the absolute areas of the internal standard (MSA, $\delta = 2.81$ ppm) from all collected ^{1}H NMR spectra. For each compound and time point, we estimated $[\text{MSA}]/[\text{MSA}]_0$ from the ratio of absolute areas. By averaging $[\text{MSA}]/[\text{MSA}]_0$ at all available irradiation times, we obtained values ranging from 0.92 ± 0.09 ($N = 7$, **S2**) to 1.00 ± 0.02 ($N = 7$, **G1**).

Furthermore, we evaluated the effect of MSA on methanol production and substrate degradation kinetics by irradiating two solutions of **G2** ($\approx$ 1 mM in D_2O), one containing MSA (0.475 mM) and one without the internal standard. Results reported in Figure S4A indicate no measurable effect of MSA on the photochemical production of methanol. Under these conditions, we calculated pseudo-first-order degradation rate constants of (0.360 ± 0.014) h^{-1} and (0.383 ± 0.021) h^{-1} in the absence and presence of MSA, respectively, implying that also **G2** kinetics are unaffected by the presence of MSA.

Methanol stability To confirm that CH_3OH is an end-product during ^{1}H NMR experiments, we followed the decay of ^{13}C-labeled methanol (Sigma-Aldrich, 99 atom% ^{13}C) in the presence and absence of **G2** ($[\mathbf{G2}]_0 = 1.08$ mM in D_2O, 6 UV lamps), which was used as a source of reactive intermediates. The ^{1}H NMR spectrum of ^{13}C-labeled methanol consists of a doublet centered at 3.36 ppm with a large coupling constant of $J = 142$ Hz.[20] Thus, the two peaks at $\delta = 3.53$ and 3.17 ppm do not overlap with the $^{12}CH_3OH$ singlet at $\delta = 3.36$ ppm, and neither they overlap with **G2** photooxidation products ($\delta > 3.8$ ppm). By plotting the relative areas of ^{13}C-labeled methanol as a function of time, we obtained pseudo-first-

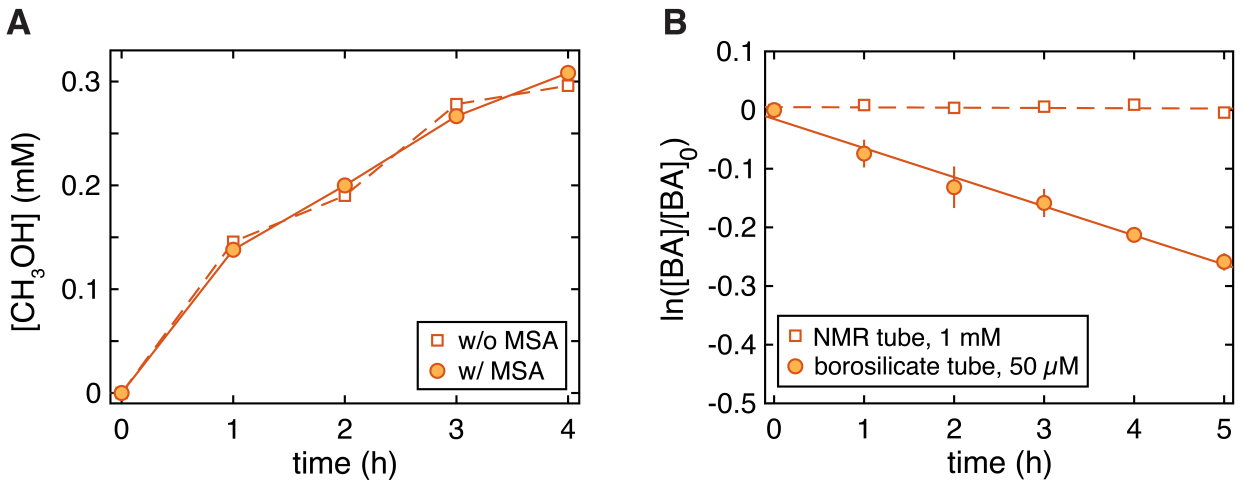

Figure S4: **A** Methanol photoproduction kinetics from **G2** ($[\mathbf{G2}]_0$ = 1.44 mM in D_2O, 6 UV lamps) in the presence and absence of the internal standard (MSA, 0.48 mM). Each point is a single determination. **B** Comparison of benzoate (BA) degradation kinetics when irradiated (6 UV lamps) in the presence of 1 mM of **G2** in a NMR tube (open squares) or in the presence of 50 μM of the same compound in a borosilocate test tube (filled circles). Each point is the average of a duplicate experiment, and error bars are the variance (within the symbol when not visible). Lines are linear regressions.

order decay rate constants of (0.020 ± 0.016) h^{-1} and (0.028 ± 0.009) h^{-1} in the absence and presence of **G2**, respectively, with $area_{end}/area_0 = 0.92$ in both cases. The negligible difference between the two conditions indicates that CH_3OH is stable during UV irradiation under the conditions of ^1H NMR experiments (i.e., in the presence of millimolar amounts of substrates).

To substantiate this result, we quantified $[OH^\bullet]_{ss}$ in a 1 mM solution of **G2** placed into an NMR tube. In this experiment, we simultaneously irradiated two solutions (6 UV lamps): one contained 1 mM of **G2** in D_2O and was placed in an NMR tube; the other was prepared with 50 μM of the same substrate in nanopure water and was irradiated in a borosilicate test tube. Each solution was also amended with benzoate (BA, 10 μM) as the $OH^\bullet$ probe. Similar to other ^1H NMR experiments, the solution in the NMR tube was shaken every 30 min to assure mixing. At each time point, we collected 150 μL aliquots and we quantified BA via UPLC. Figure S4B unambiguously indicates that $OH^\bullet$ are not produced (or, if produced, they are below the method's detection limit) during ^1H NMR experiments (open squares), while their concentration is higher in the diluted solutions used to quantify CO (filled circles, $[OH^\bullet]_{ss} = 2.3 \times 10^{-15}$ M).

Acetone control During UV irradiation, we sometimes observed the formation of a singlet at $\delta = 2.23$ ppm, which we identified as acetone upon addition of an authentic standard. Due to lack of reproducilibity and the fact that acetone was used to clean NMR tubes and caps, we concluded that its production must be an experimental artifact. To confirm that the presence of trace amounts of acetone does not influence Y_{CH3OH} values, we simultaneously irradiated two solutions of **G2** ($\approx$ 1 mM in D_2O, 6 UV lamps), one unamended and one spiked with acetone (0.5 mM). In the two cases, we obtained $Y^{\mathrm{acetone}}_{\mathrm{CH3OH}}/Y_{\mathrm{CH3OH}} = 1.08 \pm 0.06$ while pseudo-first-order degradation rate constants of **G2** were $k^{\mathrm{acetone}}_{obs,\mathbf{G2}}/k_{obs,\mathbf{G2}} = 1.05 \pm 0.09$. These results suggest that small amounts of acetone are unlikely to affect our experimental results.

S6.3 Hydroxyl radicals

Dark control We irradiated for 6 h (6 UV lamps) solutions containing **G2** (50 μM) and benzoate (BA, 10 μM) in nanopure water either covered in Al foil or uncovered, and we quantified BA depletion via UPLC. For the light exposed sample, we measured $k_{obs,\mathrm{BA}} = (0.050 \pm 0.004)$ h^{-1}, while for the covered sample we obtained $k_{obs,\mathrm{BA}} = -(0.0003 \pm 0.0024)$ h^{-1}. Thus, BA degradation does not occur in the absence of light.

Direct photolysis control We further confirmed that BA does not degrade via direct photolysis by irradiating (6 UV lamps) a solution of benzoate (10 μM) in nanopure water. We obtained $k_{obs,\mathrm{BA}} = -(1.4 \pm 0.2) \times 10^{-3}$ h^{-1} and $[\mathrm{BA}]_{end}/[\mathrm{BA}]_0 = 1.008$, confirming that benzoate is photochemically stable under our conditions.

This result was further corroborated by detecting the formation of $\mathrm{OH}^\bullet$ products during UV irradiation of a 1 mM solution of BA in nanopure water. In agreement with the previous finding, we did not detect *m*- and *o*-hydroxybenzoic acid (*m*HBA and *o*HBA), while we observed a small production of *p*-hydroxybenzoic acid (*p*HBA; Figure S19I). The amount of *p*HBA is considerably smaller than for **H1** (i.e., 0.13 vs 0.50 μM after 6 h), which is the compound that generated the lowest amount $\mathrm{OH}^\bullet$ during experiment using 1 mM BA.

Isopropylic alcohol control on BA depletion To confirm that BA degradation in the presence of lignin model compounds is caused solely by $\mathrm{OH}^\bullet$, we repeated the benzoate depletion experiments (10 μM) in the presence of 1% (v/v) isopropylic alcohol (IPA), a known hydroxyl radical quencher. Given its second-order rate constant with $\mathrm{OH}^\bullet$ of 1.9×10^9 M^{-1} s^{-1},[21] we expected 99.98% of the $\mathrm{OH}^\bullet$ to be quenched in the presence of 1% IPA. In

agreement with our prediction, we observed suppression of BA depletion for all lignin model compounds (Figure S18, empty diamonds).

Formation of BA degradation products As an additional proof that $OH^{\bullet}$ are being generated, we irradiated lignin model compounds in the presence higher concentrations of benzoate (1 mM) to detect the formation of the three $OH^{\bullet}$ products, i.e., *p*HBA, *m*HBA, and *o*HBA. Figure S19 shows that each model compound can produce *p*HBA and *o*HBA. Each molecule also produced *m*HBA, but it could not be quantified reliably as this isomer always overlapped with substrate's degradation products. Remarkably, BA products also formed upon irradiation of **H1** and **GD2**, the two compounds that did not induce BA decay (Figure S18A and F), but they did not form in appreciable amounts when BA was irradiated alone (Figure S19I). Based on this result, we concluded that all lignin model compounds form $OH^{\bullet}$, and that the detection limit for the approach based on BA depletion is $[OH^{\bullet}]_{ss} \approx 2 \times 10^{-16}$ M.

We highlight that only *p*HBA concentration grows linearly as a function of time because *m*HBA and *o*HBA are not stable under UV light, resulting in growth-and-decay kinetics. Specifically, under our experimental conditions, we measured $k_{obs,p\mathrm{HBA}} = (0.0026 \pm 0.0002)$ $\mathrm{h}^{-1} \ll k_{obs,m\mathrm{HBA}} = (0.533 \pm 0.008)$ $\mathrm{h}^{-1} < k_{obs,o\mathrm{HBA}} = (1.28 \pm 0.02)$ h^{-1}.

Table S1: Details UPLC methods for lignin model compounds, benzoate (BA) and its $OH^{\bullet}$-products. Vanillic acid (**G3**; $\geq$ 97%, Fluka) was employed only to confirm the correlation between CO production and parent compound degradation. Eluents: A = 90% (acetate buffer pH 6) + 10% ACN; B = 90% (0.1% formic acid) + 10% ACN; C = 100% ACN. For all lignin model compound, the column temperature was not set; for BA and its products, it was set to 50°C. [a] B = 0.1% formic acid.

	%A	%B	%C	Flow rate (mL min^{-1})	Detection wavelength (nm)	r.t. (min)
α-Alcohols						
H1	90	–	10	0.15	230	4.7
G1	90	–	10	0.15	230	5.2
S1	90	–	10	0.15	230	5.1
GD1	60	–	40	0.20	280	2.0
GD2	60	–	40	0.20	280	2.4
α-Ketones						
H2	50	–	50	0.20	280	2.2
G2	50	–	50	0.20	280	2.3
S2	50	–	50	0.20	280	2.2
Carboxylic acids						
G3	–	90	10	0.15	245	5.9
BA	–	75[a]	25	0.13	230	7.8
***p*HBA**	–	75[a]	25	0.13	255	3.7
***m*HBA**	–	75[a]	25	0.13	230	4.1
***o*HBA**	–	75[a]	25	0.13	230	8.7

S7 Additional details CO samples and data analysis

S7.1 Instrument details

To quantify headspace CO concentrations in the 20 mL serum vials, we used a portable gas chromatograph (GC) equipped with a flame ionization detector (FID) and a methanizer (Model 8610, SRI instruments, Menlo Park CA). Gasses were separated over a 2.7 m Hayesep D column heated at 40°C using N_2 as the carrier gas (25 psi). The gas flow was directed to a methanizer, which was operated at an hydrogen pressure of 24 psi, and then to the FID (kept at 300°C). Under these conditions, CO eluted at 1.82 min, while CO_2, which was also a reaction product, eluted at 4.27 min. Using the standard deviation of repeated measurements of the lowest concentration standard, we obtained a detection limit for CO of 0.5 ppm.

For headspace sampling, we used a 10 mL gas-tight disposable plastic syringe (Omnifix Luer Lock Solo, Braun) equipped with a 3-way valve (Discofix C, Braun) and a disposable needle (Sterican, Braun, 0.60×25 mm, 23 G $\times$ 1"). The 20 mL serum vials were first allowed to equilibrate to room temperature, then the internal pressure ($p_{tot,hs}$) was measured with a manometer. The syringe was first flushed with $\approx$ 1 mL of gas sample, then $\approx$ 6 mL of gas sample was manually injected into the instrument. The GC analysis yielded headspace CO concentrations ($p_{\mathrm{CO},hs}$, in ppm) that we used to obtain dissolved CO concentrations in the experimental headspace-free test tubes ([CO], in μM) as described in the following section. Headspace CO concentrations in the irradiated solutions were between 3.8 and 50 ppm. Values before irradiation were typically below detection limit ($0 - 0.3$ ppm).

S7.2 Data analysis

We obtained dissolved CO concentrations in the headspace-free test tubes ([CO], in μM) via eq (S1).

$$[\mathrm{CO}] = \frac{n_{\mathrm{CO},aq} + n_{\mathrm{CO},hs}}{V_{aq}}\,, \tag{S1}$$

where V_{aq} is the volume of liquid in the 20 mL serum vial (obtained gravimetrically; $\approx$ 6 mL, see Section S4.2), while $n_{\mathrm{CO},aq}$ and $n_{\mathrm{CO},hs}$ are the moles of CO in the serum vials' aqueous phase and headspace, respectively. This equation assumes that the total moles of CO of the $\approx$ 6 mL of samples withdrawn from the headspace-free test tube (i.e., $[\mathrm{CO}]V_{aq}$) equate the total moles of CO in the serum vial, where the presence of a headspace allow CO to partition between aqueous and gas phase.

We used the ideal gas law to convert the measured headspace CO vapor pressure ($p_{CO,hs}$, in ppm) into $n_{CO,hs}$ via eq (S2).

$$n_{CO,hs} = \frac{p'_{CO,hs} V_{hs}}{RT}, \tag{S2}$$

where $p'_{CO,hs}$ is the measured CO headspace vapour pressure expressed in atm, V_{hs} is the headspace volume of the serum vial (in L), $R = 0.082$ L atm mol^{-1} K^{-1} is the gas constant, and T (in K) is the air temperature at the time of the GC measurement. $p'_{CO,hs}$ was obtained from the measured headspace concentration ($p_{CO,hs}$, in ppm) as $p'_{CO,hs} = p_{CO,hs} \cdot p_{tot,hs}/1013$, where $p_{tot,hs}$ (in mbar) is the total gas pressure in the serum vial before GC measurement (measured with a manometer) and 1013 is a conversion factor. V_{hs} was calculated as $V_{vial} - V_{aq}$ using the exact aqueous volumes obtained gravimetrically, and was ≈ 14 mL.

For the aqueous phase, we obtained $n_{CO,aq}$ via Henry's law (eq (S3)) using the calculated CO moles in the headspace ($n_{CO,hs}$, eq (S2)), the volume of liquid in the serum vial (V_{aq}), the headspace volume of the same vial (V_{hs}), and the Henry's constant for CO (K_{CO}, unitless; defined here as $[CO]_{gas}/[CO]_{liquid}$).

$$n_{CO,aq} = \frac{n_{CO,hs} V_{aq}}{K_{CO} V_{hs}} \tag{S3}$$

We adjusted K_{CO} for variations in air temperature according to Fry et al.[22] Specifically, we fitted Fry et al's empirical K_{CO} values with a linear function, resulting in $K_{CO}(T) = 0.568 \cdot T\ [^\circ C] + 29.01$. At our experimental temperatures ($T = 19 - 23^\circ$C), K_{CO} was between 39 and 42.

By combining equations S1 − S3, one obtains the following expression (eq 3 in the main text).

$$[CO] = \frac{p'_{CO,hs}}{RT}\left(\frac{V_{hs}}{V_{aq}} + \frac{1}{K_{CO}}\right) \tag{S4}$$

S7.3 Characterization of the rubber stopper interference

A solution containing nanopure water was irradiated in a headspace-free setup (6 UV lamps) alongside a solution containing **H1** (50 μM). GC-FID analyses confirmed that CO production from **H1** was approximately comparable to the amount produced by nanopure water alone, as $[CO]_{6h} = (1.32 \pm 0.24)$ μM (water, $N = 6$) and (1.44 ± 0.33) μM (**H1**, $N = 3$) (Figure S5A). Overall, the value for **H1** was slightly (but not statistically) higher than the value obtained with nanopure water alone (i.e., $[CO]_{6h}^{water}/[CO]_{6h}^{\mathbf{H1}} = 0.85 \pm 0.03, N = 3$). For this

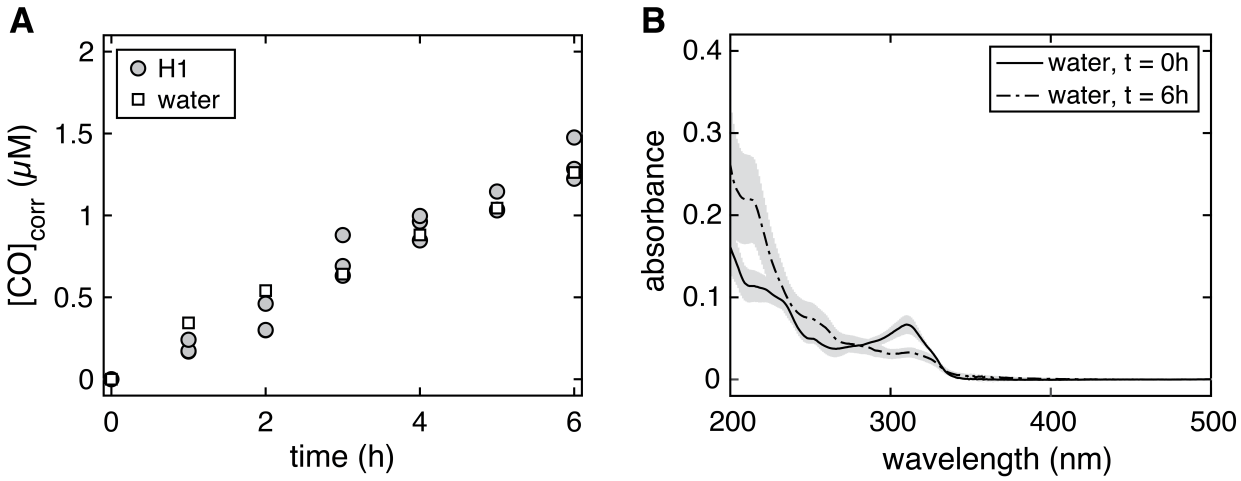

Figure S5: **A** CO photoproduction kinetics of **H1** (circles) and nanopure water (squares) during UV irradiation (6 lamps). **B** UV-vis spectra of nanopure water in contact with the rubber stopper before (continuous line) and after 6 hour of UV irradiation (dash-dot line). Grey areas are the standard deviation calculated from $3-4$ independent measurements.

reason, we used $[\mathrm{CO}]_{6\mathrm{h}}$ values for **H1**, which was measured more often than nanopure water alone, to correct 6 h CO concentrations in the calculation of Y_{CO}.

UV-vis analyses of nanopure water (after ≈ 8 h contact with the rubber stopper) before irradiation showed the presence of UV chromophores (Figure S5B), most likely organic compounds released from the rubber upon contact with the liquid. Amount and spectral features of the released compounds did not change among stoppers that received different amount of light, and was overall reproducible. After 6 h of UV irradiation, the absorption spectrum showed decreased absorbance around 300 nm (Figure S5B), suggesting photobleaching with associated production of CO.

We also conducted a test using silicone stoppers (Suba-seal silicone rubber septa, Sigma Aldrich), but the results were unsatisfactory. Silicone stoppers did not leach material in solution, as confirmed by UV-vis measurements. However, their CO background after 6 h of UV irradiation (6 lamps) was 2.8 times higher than the rubber stoppers, i.e., $[\mathrm{CO}]_{6\mathrm{h}}^{\mathrm{silicone}} = (3.22 \pm 0.32)\ \mu\mathrm{M}$, while $[\mathrm{CO}]_{6\mathrm{h}}^{\mathrm{rubber}} = (1.16 \pm 0.12)\ \mu\mathrm{M}$ ($N = 3$).

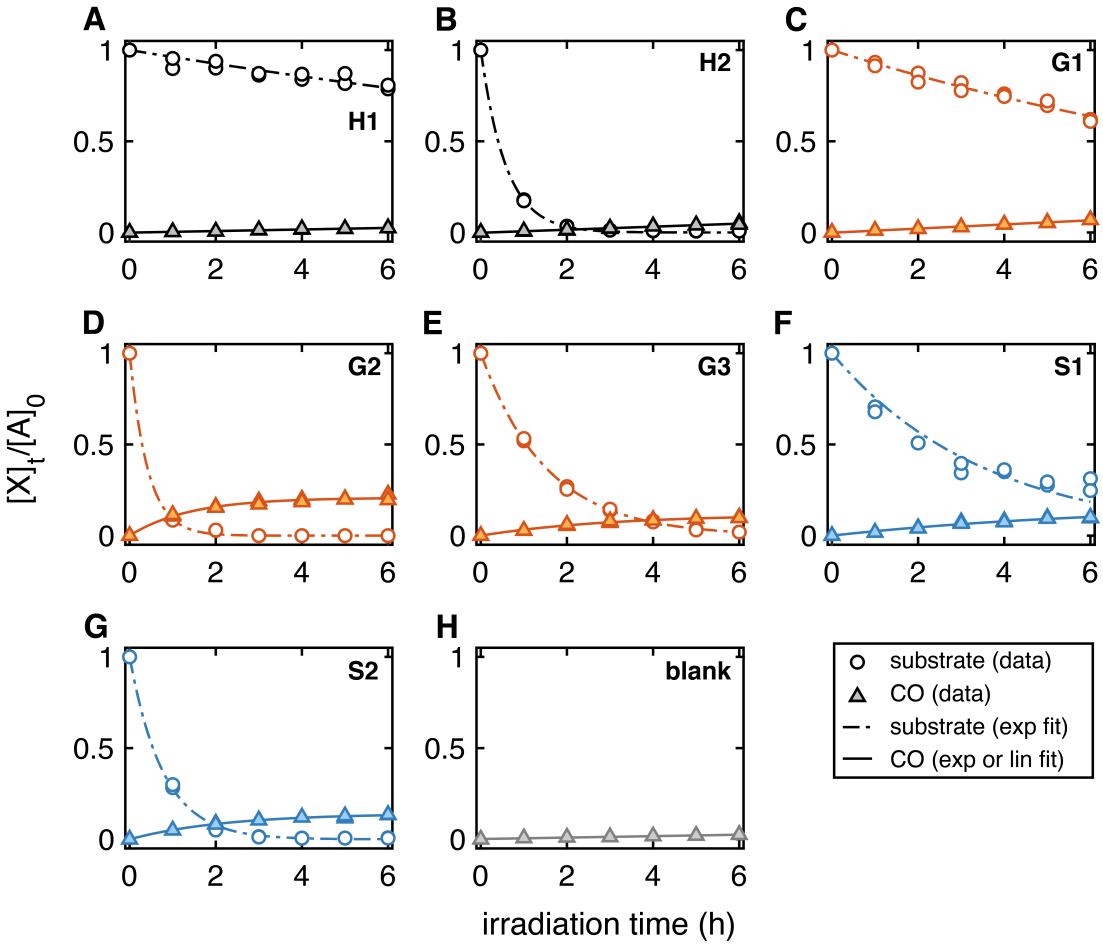

Figure S6: Parent compound degradation (open circles) and CO production kinetics (filled triangles) with 6 UV lamps ($[\text{substrate}]_0 = 50\ \mu\text{M}$). Each symbol is a single data (error not shown). Lines are exponential fits; CO data for **H1**, **H2**, **G1**, and the blank are fitted with a linear regression model (see also Table S2). CO data are not corrected for blank production. Color code: black, *p*-hydroxyphenyl derivatives; orange, guaiacyl derivatives; blue, syringyl derivatives; grey, blank control.

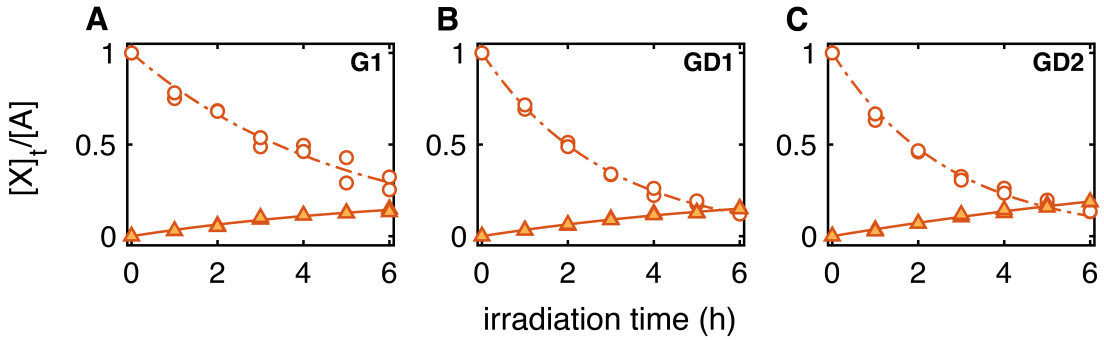

Figure S7: Parent compound degradation (open circles) and CO production kinetics (filled triangles) with 12 UV lamps ([substrate]$_0$ = 50 μM). Each symbol is a single data (error not shown), while lines are exponential fits. CO data are not corrected for blank production. Legend and color-code are the same as Figure S6.

Table S2: Numerical values of the initial substrate degradation rate (R^0_{parent}) and the initial CO production rate (R^0_{CO}) related to Figure 3 (main text). The rates were obtained from the fitting parameters as described in the main text, while the errors are calculated from error propagation. The last two columns summarize the type of fit and its R^2 referred to Figures S6 and S7.

Substrate	**# UV lamps**	$\boldsymbol{R^0_{\text{parent}}}$ **(μM h^{-1})**	$\boldsymbol{R^0_{\text{CO}}}$ **(μM h^{-1})**	**CO fit type**	**R^2**
blank	6	–	0.197 ± 0.011	linear	0.98
H1	6	1.96 ± 0.12	0.217 ± 0.009	linear	0.98
H2	6	84.9 ± 1.2	0.410 ± 0.018	linear	0.98
G1	6	3.74 ± 0.11	0.565 ± 0.013	linear	0.993
	12	10.5 ± 0.4	1.9 ± 0.8	exponential	0.98
GD1	12	19.0 ± 0.2	2.0 ± 0.6	exponential	0.992
GD2	12	15.5 ± 0.4	1.6 ± 1.0	exponential	0.99
G2	6	130 ± 4	8.1 ± 0.9	exponential	0.98
G3	6	36.7 ± 0.3	2.1 ± 0.3	exponential	0.991
S1	6	14.1 ± 0.8	1.3 ± 0.6	exponential	0.98
S2	6	72.2 ± 1.4	3.6 ± 0.3	exponential	0.993

S8 Interpreting variations in kinetic parameters: Initial vs 6h yield values

Figure S8 shows simulated variations in Y_{CO} as a function of irradiation time for a one-step (black line, full) or a two-step (grey lines, dashed) reaction. In both cases, we assumed that CO was formed in 50% yields from its precursor, i.e., that $Y_{\mathrm{CO}}^{end} = 0.5$. This graph was obtained by first simulating changes in substrate and product concentrations as a function of time using the kinetic equations detailed in the supplement of Ossola et al.[23] (values of rate constants are in the caption of Figure S8). Then, for each time point and condition, we calculated $Y_{\mathrm{CO}}^{t} = [\mathrm{CO}]_t/([\mathrm{S}]_0 - [\mathrm{S}]_t)$ (as eq 4 in the main text).

This analysis show that Y_{CO} is always constant only in one-step reactions (bold line), while $Y_{\mathrm{CO}}^{0} < Y_{\mathrm{CO}}^{t}$ if the reaction has more than one step (dashed lines). This latter relation holds valid also when the reaction kinetics appear visually similar to those of one-step reactions (in this case, when $n < 0.2$). The fact that, in our experiments, $Y_{\mathrm{CO}}^{0}(= 0.057) < Y_{\mathrm{CO}}^{6h}(= 0.112 - 0.176)$ suggests that CO is not formed in one step from lignin model compounds, but rather that it is a second generation product. This conclusion is in agreement with the proposed mechanism.

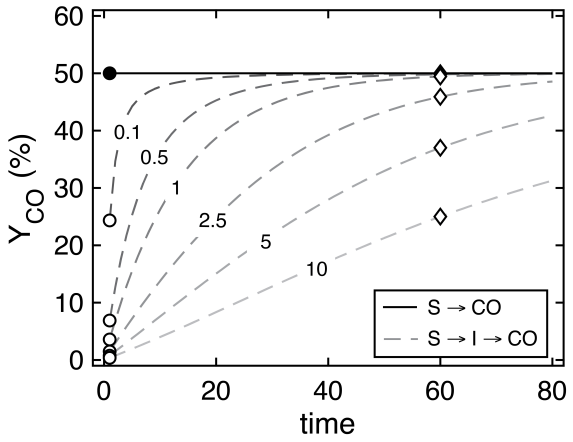

Figure S8: Simulated trend of Y_{CO} as a function of time for one-step ($\mathrm{S} \rightarrow \mathrm{CO} + \mathrm{P}'$, filled line) and two-step reactions ($\mathrm{S} \rightarrow \mathrm{I} \rightarrow \mathrm{CO} + \mathrm{P}'$, dashed lines). For the one-step reaction, we used an arbitrary first-order rate constant of $k = k^{\mathrm{CO}} + k^{\mathrm{P'}} = 0.075$ time^{-1} and $Y_{\mathrm{CO}} = 0.5$. For the two-step reaction, we used $k_1 = 0.075$ time^{-1} for the first step, while, for the second step, $k_2^{\mathrm{CO}} = k_1/n$ time^{-1} (where n has several values between 0.1 and 10; marked on the graph) and $k_2^{\mathrm{P'}} = k_2^{\mathrm{CO}}$. Circles and diamonds highlight Y_{CO} values for $t = 0$ and 60, respectively.

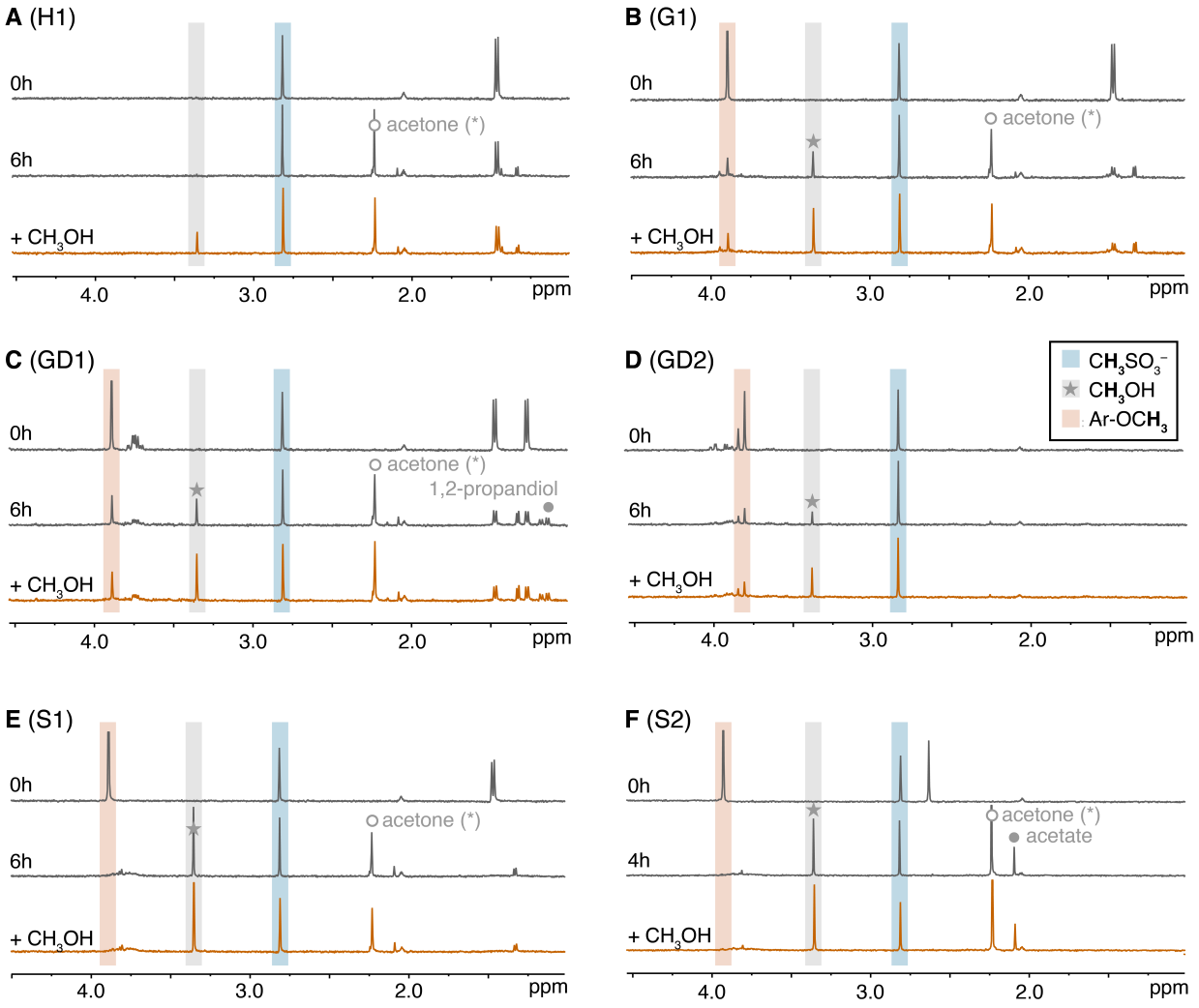

Figure S9: ^{1}H NMR spectra of lignin model compounds during 6 h (α-alcohols) or 4 h (α-ketones) of UV irradiation ([substrate]$_0$ $\approx$ 1 mMin D_2O, 6 UV lamps; dark grey traces). At the end of the experiment, we added methanol (+ 0.18 mM) to confirm its occurrence as a reaction product (orange traces). Grey areas identify CH_3OH (δ = 3.36 ppm), blue areas denote the internal standard ($CH_3SO_3^-$, δ = 2.81 ppm), and orange areas identify the Ar-OCH_3 protons of the parent compound (see also legend in panel D). Additional relevant signals are indicated with a filled circle (acetate, $\delta = 2.03 - 2.08$ ppm (s) or 1,2-propanediol, δ = 1.16 ppm (d)) or an empty circle (acetone, δ = 2.23 ppm). Note that acetone is not a reaction product.

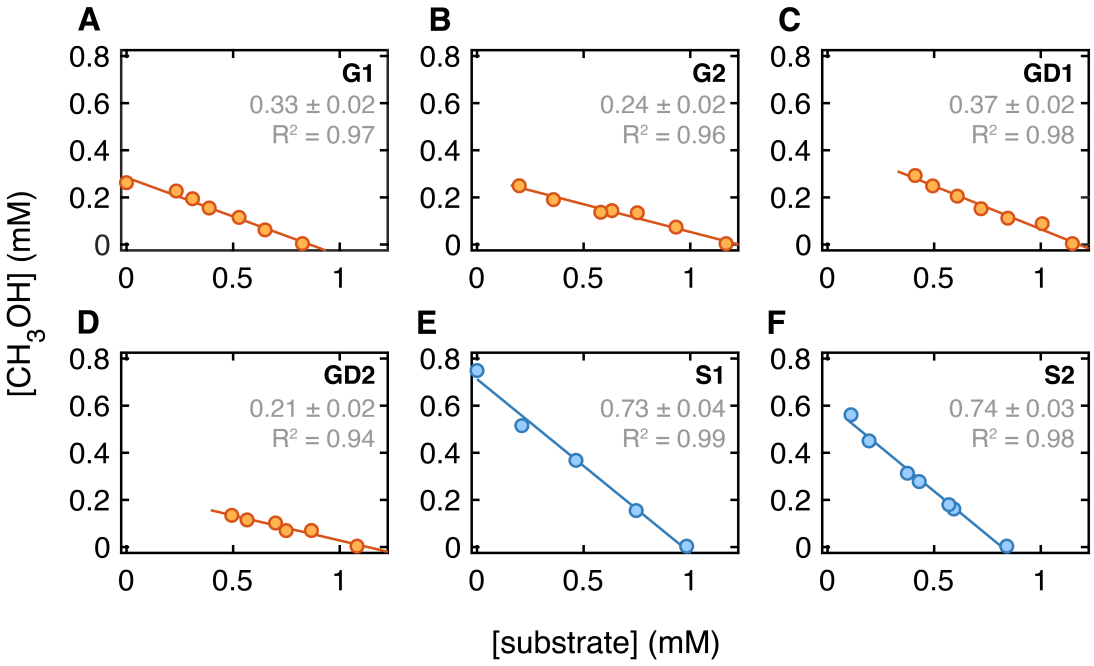

Figure S10: Plots showing the correlation between substrate and CH_3OH concentrations during ^1H NMR experiments. Concentrations are obtained from peak areas at $\delta = 3.36$ ppm (methanol) and $\delta = 3.89 - 3.95$ ppm ($ArOCH_3$). Each point is a single measurement; in grey, we report the negative slope and R^2 of the linear regression line. The negative slope represents Y_{CH3OH} and is equivalent within the experimental error to the methanol conversion efficiency reported in Table 1 (main text). Color code: orange, guaiacyl derivatives; blue, syringyl derivatives.

S9 Interpreting variations in kinetic parameters: Methanol vs substrate plots

Figure S11 presents simulated data supporting the hypothesis that methanol is formed in a formal one-step reaction from the substrates. In panel A, simulated CH_3OH and substrate concentrations (obtained as described in Text S8) are plotted against each others for one- and two-step reactions. For two-step reactions, several scenario are presented based on the value of n, the ratio between the rate constants of the first and the second step. Simulated data are then fitted to a linear regression line using either all data (blue areas) or only the data points in the range [substrate] $= 1 - 0.45$ (white areas), which are the extreme cases that we observed experimentally (see **GD2** and syringyl compounds in Figure S10). Panel B reports the negative value of the slope of the linear regression lines in panel A and its corresponding R^2 for the various values of n.

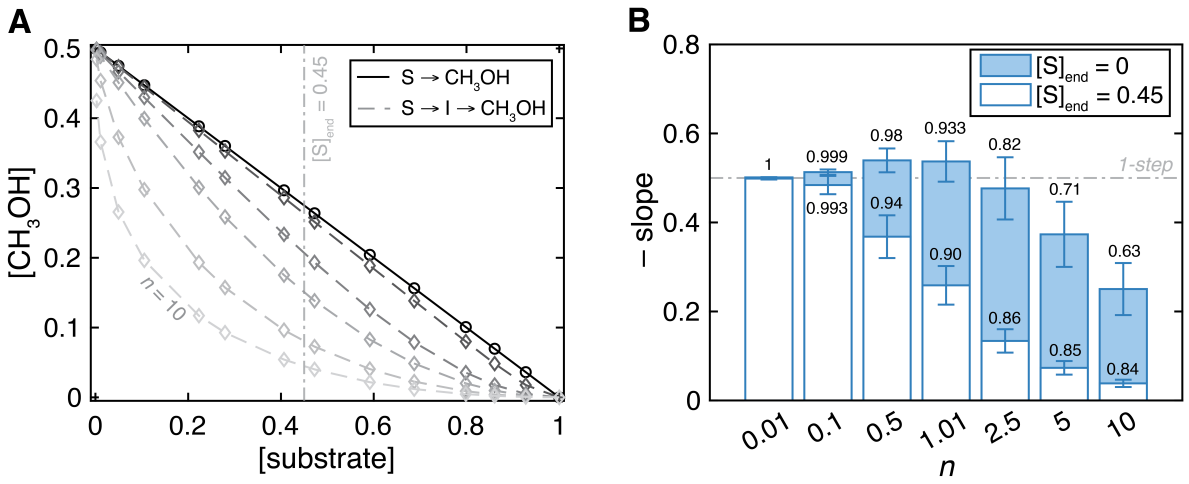

Figure S11: **A** Simulated [substrate] vs. [methanol] plots for a one-step (black, bold line and circles) or a two-step reaction (grey, dashed line and diamonds). The parameters of the kinetic equations employed in the simulations are the same described in the caption of Figure S8, with $n = 0.5 - 10$. Lines are lead lines, not regression lines, while concentrations are in arbitrary units. Data for $n = 0.01$ and 0.1 are omitted for clarity. **B** Negative slopes of the linear regression analyses of data in Figure S11A using either all data points (filled areas, $[S]_{end} = 0$) or the first data points until $[S]_{end} = 0.45$ (empty areas, marked in panel A). Error bars are the error of the slope and the numeric data are R^2 values of the linear regressions. The grey, dash-dotted line is the slope obtained for a 1-step reaction ($-$slope $= 0.5$).

This analysis supports the hypothesis that methanol is formed from the photodegradation of lignin model compounds either via a one-step or a "formal" one-step reaction - i.e., a two-

step reaction with $n \leq 0.1$. In fact, we obtained experimental $R^2 = 0.99 - 0.94$ and, most importantly, negative slope values in excellent agreement with the Y_{CH3OH} values reported in Table 1 (main text and Figure S10).

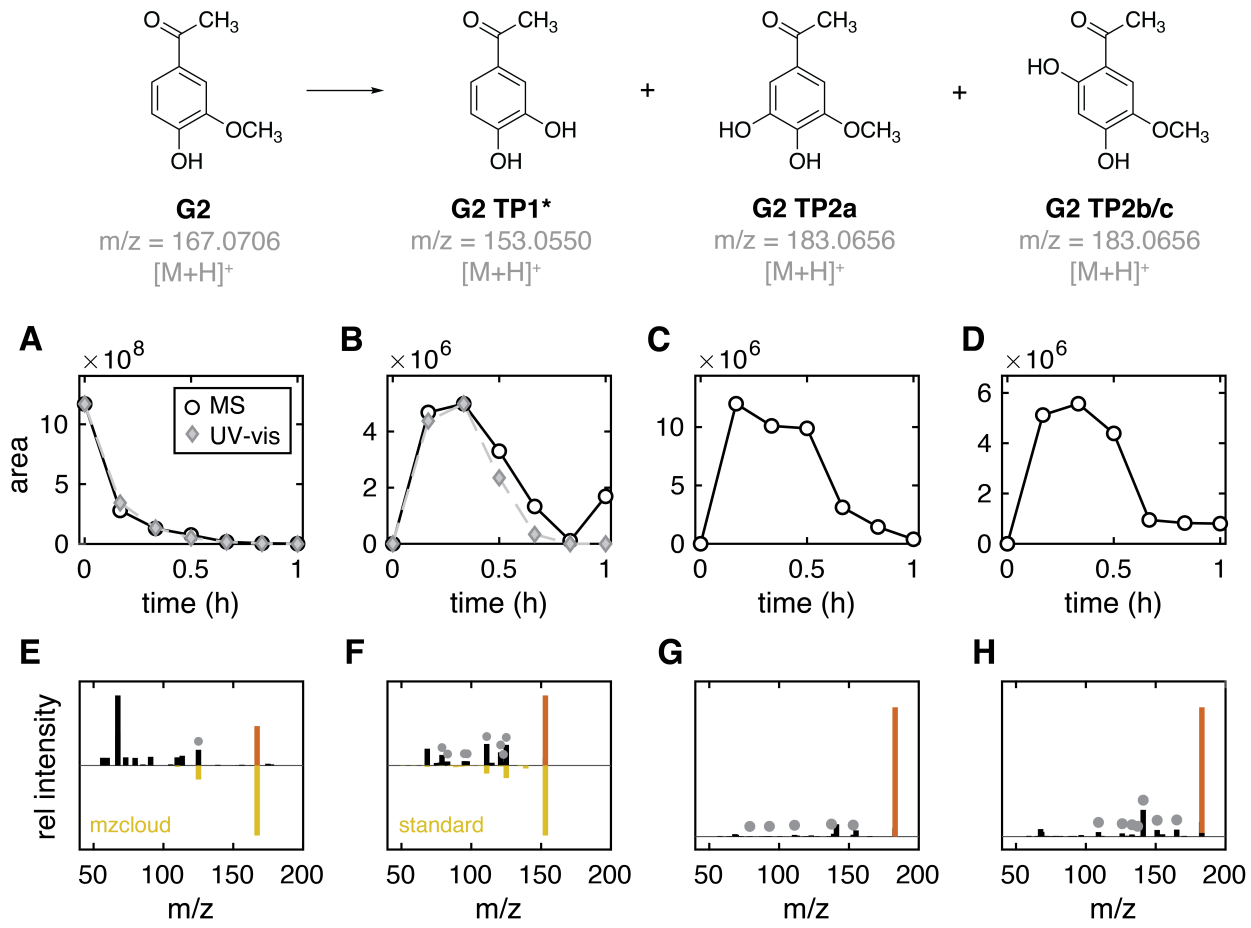

Figure S12: **Top** Chemical structures, m/z values, and ion type detected via LC-HRMS during UV irradiation of **G2** (12 UV lamps). Note that TP2b/c (m/z = 183.0656) can be either of the two isomers (i.e., 2-OH or 6-OH; only the latter structure is shown); the third isomer (i.e., TP2a) was identified based on retention time similarity with S2 TP1 (see Table S3). **Bottom** Kinetic traces and MS^2 spectra (NCE = 30) relative to chemical structures and m/z values indicated above (e.g., data for **G2** are shown in panel A and E). In panel A and B, kinetics obtained via LC-HRMS (empty circles) are overlaid with values obtained via UPLC with UV-vis detection (gray diamonds; UPLC method details in Table S1). In panels E – H, orange bars highlight the unfragmented molecule, while circles mark fragments obtained using [M] as the input in MetFrag. Yellow MS^2 spectra are comparison with experimental data from mzcloud (panel E) or experimental data collected using a commercial standard (panel F).

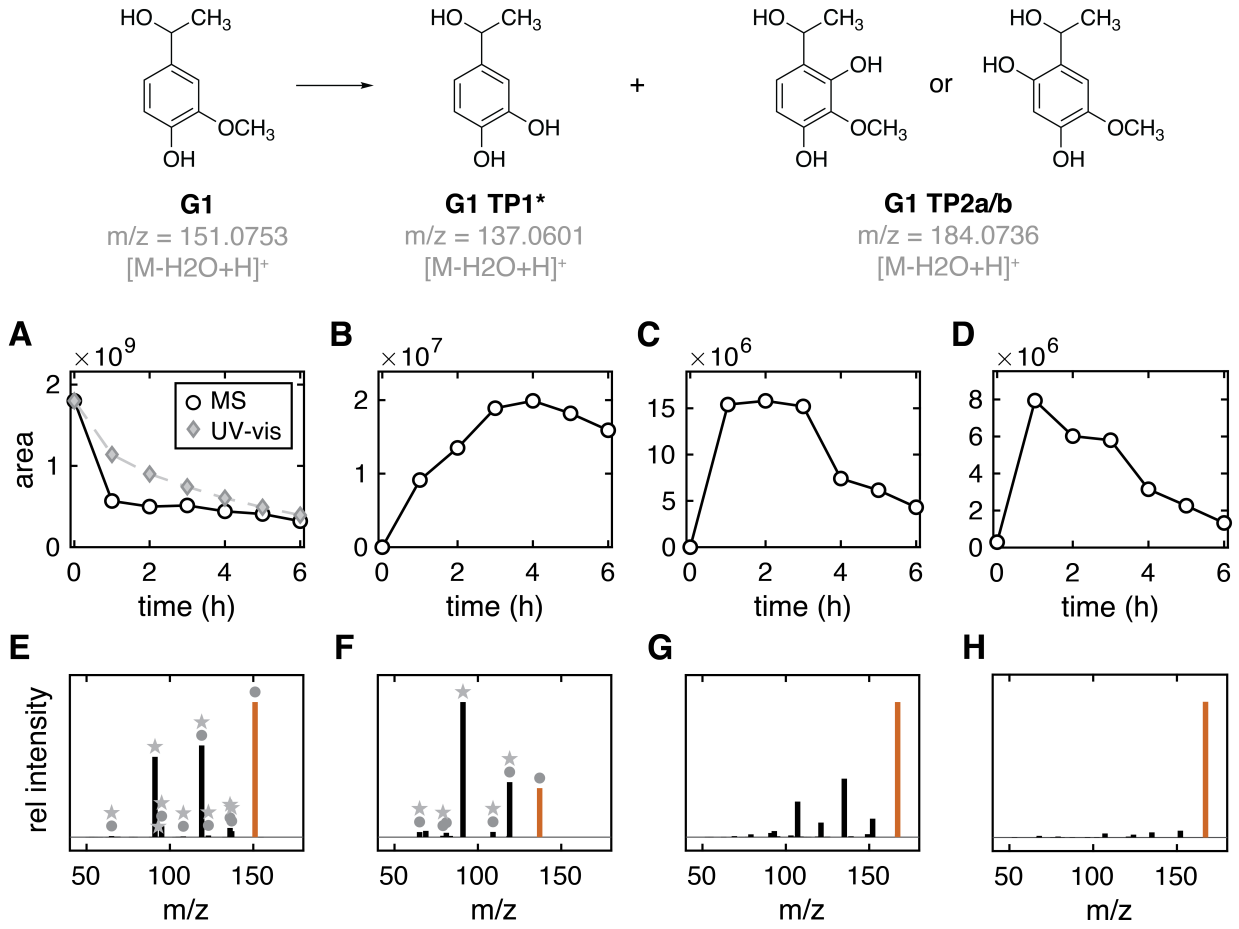

Figure S13: **Top** Chemical structures, m/z values, and ion type detected via LC-HRMS during UV irradiation of **G1** (12 UV lamps). Note that TP2 (m/z = 184.0736) can be either of the two isomers; the third isomer (i.e., 5-OH substitution) is excluded based on the difference in retention time between TP2a/b and S1 TP1. **Bottom** Kinetic traces and MS^2 spectra (NCE = 30) relative to chemical structures and m/z values indicated above (e.g., data for **G1** are shown in panel A and E). In panel A, kinetics obtained via LC-HRMS (empty circles) are overlaid with values obtained via UPLC with UV-vis detection (gray diamonds; method in Table S1). In panels E – H, orange bars highlight the unfragmented molecule, circles mark fragments obtained using [M] as the input in MetFrag, while stars mark fragments using [M−H2O] as the input (where water is lost from the α-alcohol functionality).

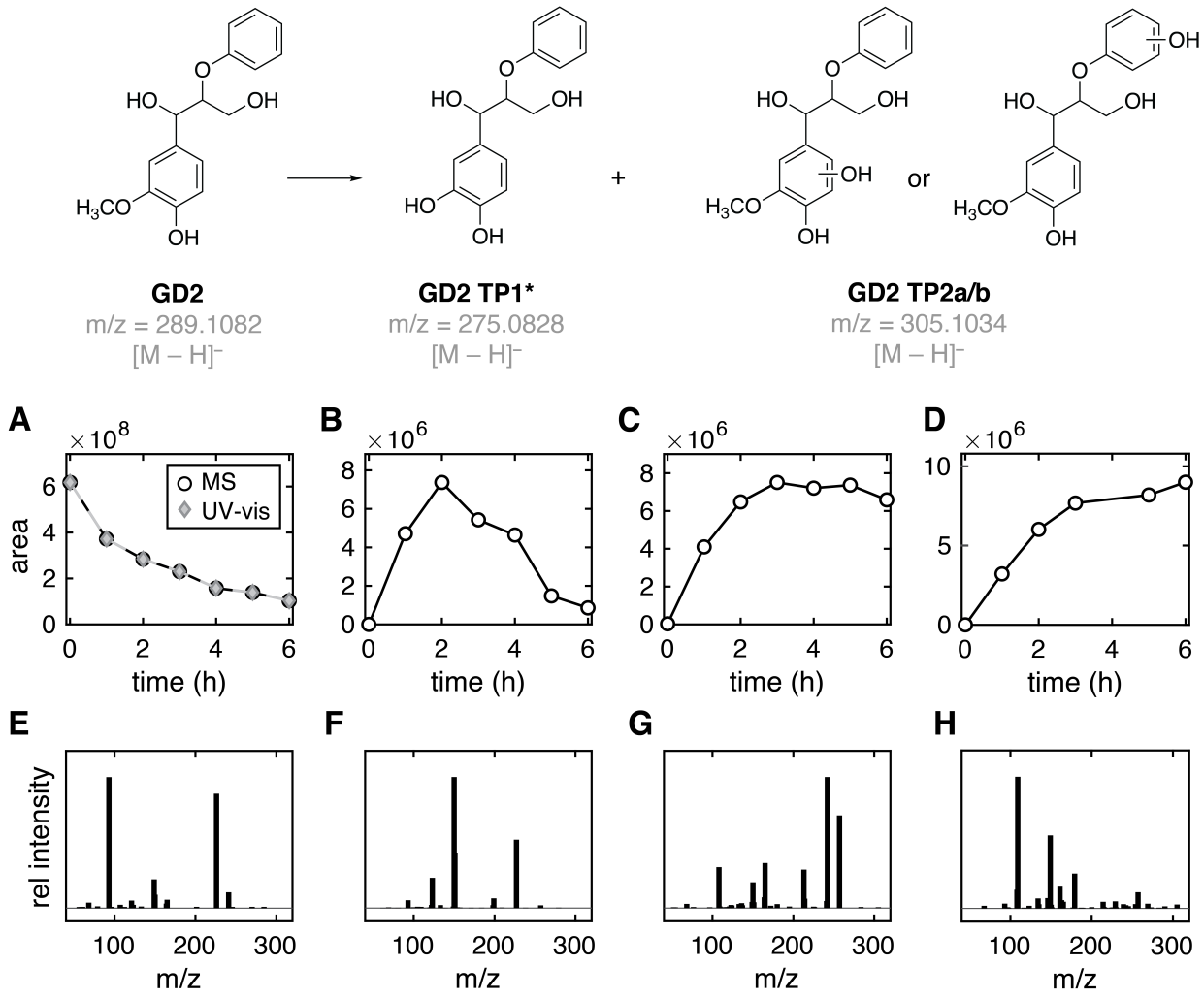

Figure S14: **Top** Chemical structures, m/z values, and ion type detected via LC-HRMS during UV irradiation of **GD2** (12 UV lamps). Note that TP2 (m/z = 305.1034) can be either of the two type of isomers, i.e., **GD2** hydroxylated on the guaiacyl ring (left) or on the *p*-hydroxyphenyl ring (right). We also detected a broad signal at m/z = 321.0892 relative to the species **GD2** + 2OH, but we could not obtain a clear MS^2 for this TP (see Table S3). **Bottom** Kinetic traces and MS^2 spectra (NCE = 30) relative to chemical structures and m/z values indicated above (e.g., data for **GD2** are shown in panel A and E). In panel A, kinetics obtained via LC-HRMS (empty circles) are overlaid with values obtained via UPLC with UV-vis detection (gray diamonds; method in Table S1). All compounds were also detected in ESI(+) mode as $[M + Na]^+$ adducts (data not shown).

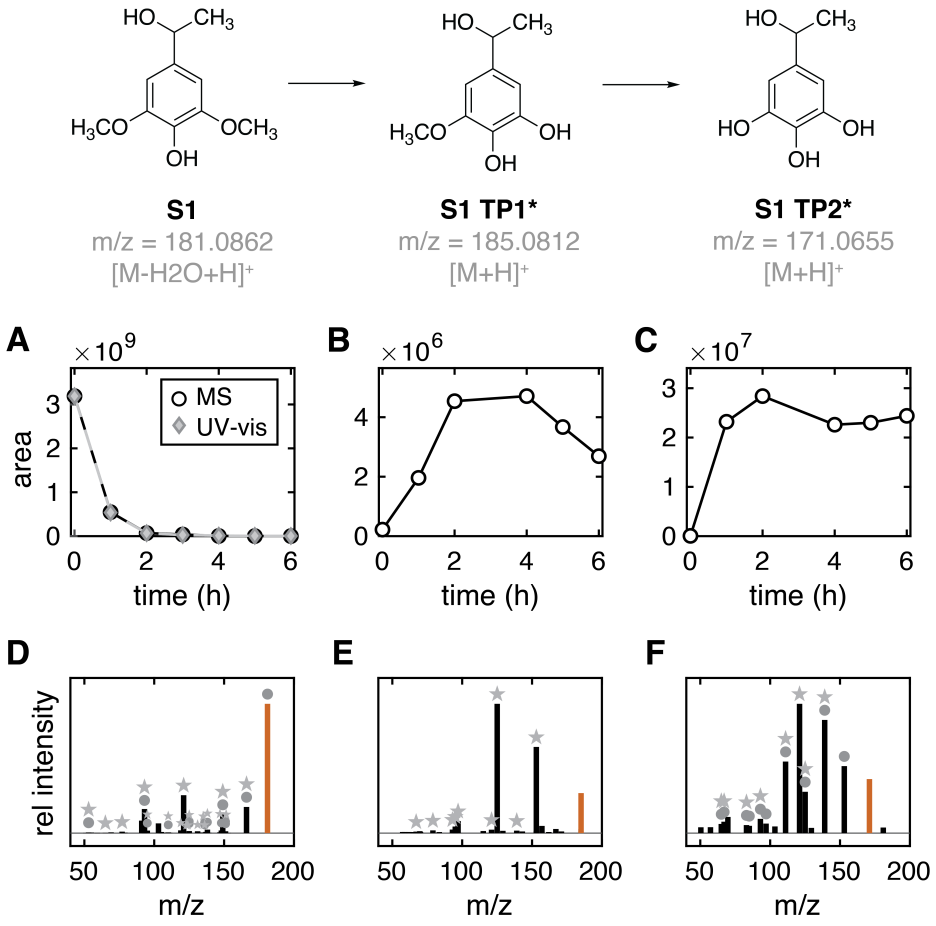

Figure S15: **Top** Chemical structures, m/z values, and ion type detected via LC-HRMS during UV irradiation of **S1** (12 UV lamps). **Bottom** Kinetic traces and MS^2 spectra (NCE = 30) relative to chemical structures and m/z values indicated above (e.g., data for **S1** are shown in panel A and D). In panel A, kinetics obtained via LC-HRMS (empty circles) are overlaid with values obtained via UPLC with UV-vis detection (gray diamonds; method in Table S1). In panels D – F, orange bars highlight the unfragmented molecule, circles mark fragments obtained using [M] as the input in MetFrag, while stars mark fragments using [M − H2O] as the input (where water is lost from the α-alcohol functionality).

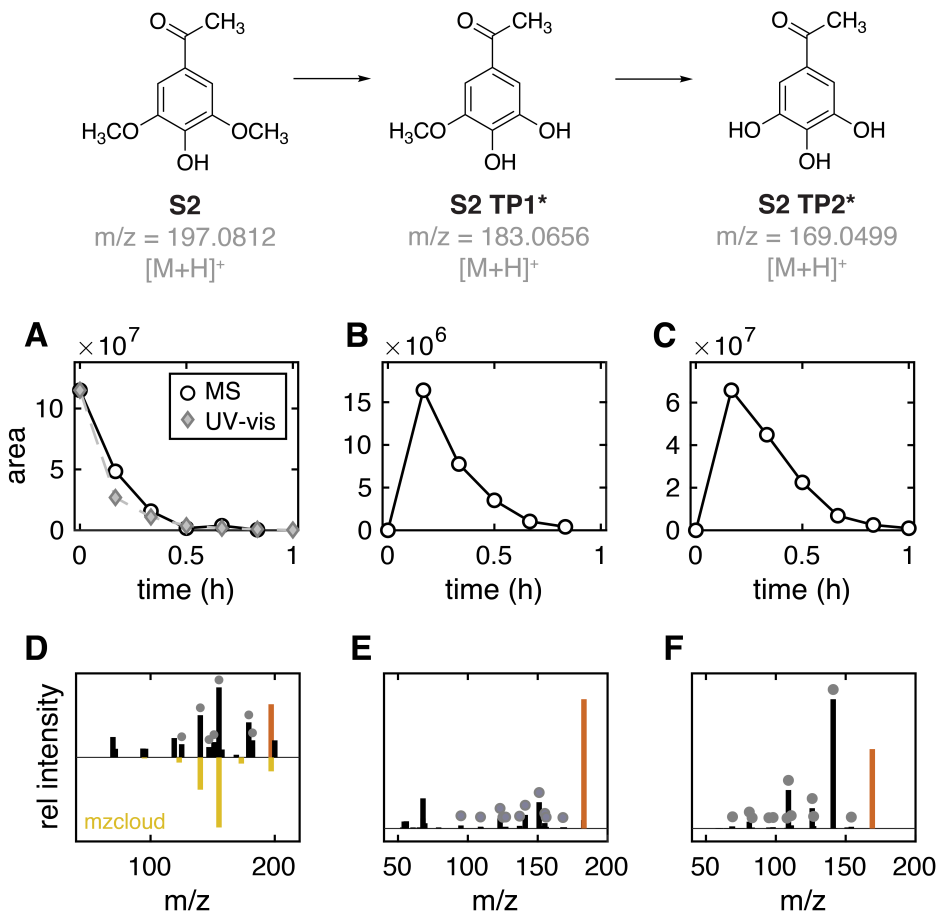

Figure S16: **Top** Chemical structures, m/z values, and ion type detected via LC-HRMS during UV irradiation of **S2** (12 UV lamps). **Bottom** Kinetic traces and MS^2 spectra (NCE = 30) relative to chemical structures and m/z values indicated above (e.g., data for **S2** are shown in panel A and D). In panel A, kinetics obtained via LC-HRMS (empty circles) are overlaid with values obtained via UPLC with UV-vis detection (gray diamonds; method in Table S1). In panels D – F, orange bars highlight the unfragmented molecule, while circles mark fragments obtained using [M] as the input in MetFrag. The yellow MS^2 spectrum is experimental data from mzcloud (panel D).

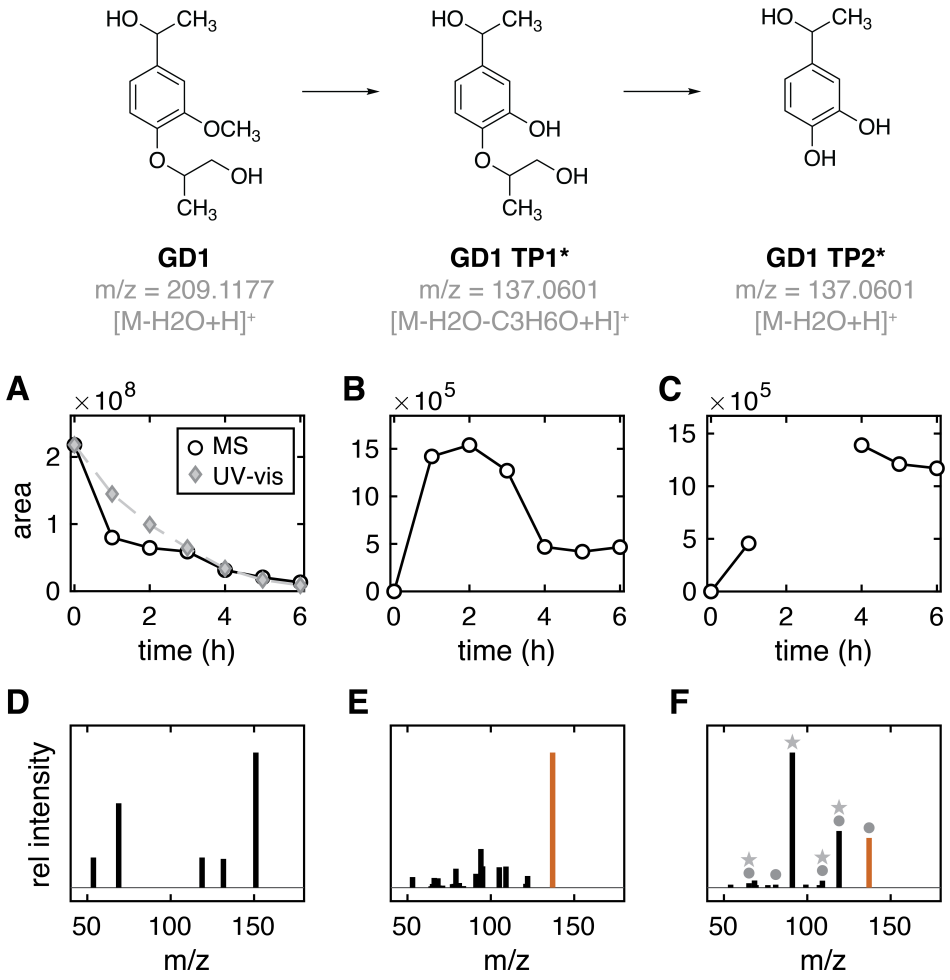

Figure S17: **Top** Chemical structures, m/z values, and ion type detected via LC-HRMS during UV irradiation of **GD1** (12 UV lamps). Note that TP1 and TP2 have the same m/z but different retention time and MS^2. We hypothesized that TP1 loses its aliphatic group in *para* (i.e., C_3H_7O) in the ion source, and it is therefore detected at $m/z = 137.0601$. On the other hand, TP2 has the same r.t. and characteristic fragment ions (m/z = 137, 119, 91) of G1 TP1 (Figure S13F). **Bottom** Kinetic traces and MS^2 spectra (NCE = 30) relative to chemical structures and m/z values indicated above (e.g., data for **GD1** are shown in panel A and D). In panel A, kinetics obtained via LC-HRMS (empty circles) are overlaid with values obtained via UPLC with UV-vis detection (gray diamonds; method in Table S1). In panels D – F, orange bars highlight the unfragmented molecule, circles mark fragments obtained using [M] as the input in MetFrag, while stars mark fragments using [M − H2O] as the input (where water is lost from the α-alcohol functionality).

Table S3: Overview of photodegradation products detected via LC-HRMS.

Product ID	**Chemical formula**	**Exact mass**	**ESI type**	**Ion type**	***m/z***	**r.t. (min)**	**MS^2**	**Confidence level**
Substrate: **G1**								
TP1*	C8H10O3	154.0630	+	$[M - H2O + H]^+$	137.0601	9.4	Fig. S13F	2
TP2a	C9H12O4	184.0736	+	$[M - H2O + H]^+$	167.0701	10.0	Fig. S13G	3
TP2b	C9H12O4	184.0736	+	$[M - H2O + H]^+$	167.0702	12.5	Fig. S13H	3
Substrate: **G2**								
TP1*	C8H8O3	152.0473	+	$[M + H]^+$	153.0550	11.2	Fig. S12F	1
TP2a	C9H10O4	182.0579	+	$[M + H]^+$	183.0656	11.5	Fig. S12G	2
TP2b	C9H10O4	182.0579	+	$[M + H]^+$	183.0656	13.7	Fig. S12H	2
Substrate: **GD1**								
TP1*	C11H16O4	212.1049	+	$[M - H2O - C3H6O + H]^+$	137.0601	12.5	Fig. S17E	$3 - 4^{\ddagger}$
TP2*	C8H10O3	154.0630	+	$[M - H2O + H]^+$	137.0601	9.4	Fig. S17F	2
Substrate: **GD2**								
TP1*	C15H16O5	276.0998	−	$[M - H]^-$	275.0828	12.2	Fig. S14F	3
TP2a	C16H18O6	306.1103	−	$[M - H]^-$	305.1033	10.1	Fig. S14G	3
TP2b	C16H18O6	306.1103	−	$[M - H]^-$	305.1034	13.0	Fig. S14H	3
TP3	C16H18O7	322.1053	−	$[M - H]^-$	321.0982	$12.7 - 14.0^{\dagger}$	N/A	4
Substrate: **S1**								
TP1*	C9H12O4	184.0736	+	$[M + H]^+$	185.0812	11.4	Fig. S15E	2
TP2*	C8H10O4	170.0579	+	$[M + H]^+$	171.0655	10.6	Fig. S15F	$2 - 3^{\ddagger\ddagger}$
Substrate: **S2**								
TP1*	C9H10O4	182.0579	+	$[M + H]^+$	183.0656	11.5	Fig. S16E	2
TP2*	C8H8O4	168.0423	+	$[M + H]^+$	169.0499	10.4	Fig. S16F	2

Table S3: (continuing) Transformation products (TP) of different chemical formula are identified with increasing numbers (i.e., TP1, TP2, TP3); structural isomers are labeled with a letter (e.g., TP2a and TP2b), while TP that agree with the proposed mechanism are identified with an asterisk (e.g., TP1*). The exact mass is calculated with ChemDraw from the chemical formula, while *m/z* is the value detected during MS analyses. Experimental MS^2 (and their comparison with mzcloud spectra, when available) and relevant chemical structures are in Figures S13 – S17. The confidence level was obtained based on Schymanski et al.[24] We assigned 1 (*confirmed structure*) when we could match r.t., MS^1, and MS^2 to a reference standard; 2 (*probable structure*) when we could explain all major MS^2 fragments with *in-silico* predictions obtained with MetFrag; 3 (*tentative candidate*) if MS^2 was available but no match was found with *in-silico* predictions; 4 if only MS^1 data were available. † Broad signal observed at this *m/z*. No clear MS^2 reported. ‡ The different r.t. but same *m/z* suggests loss of a C_3H_6O fragment in the ion source. ‡‡ Good match with *in-silico* fragmentation only when the dehydrated molecule is used as the input (water is lost from the α-carbon functionality).

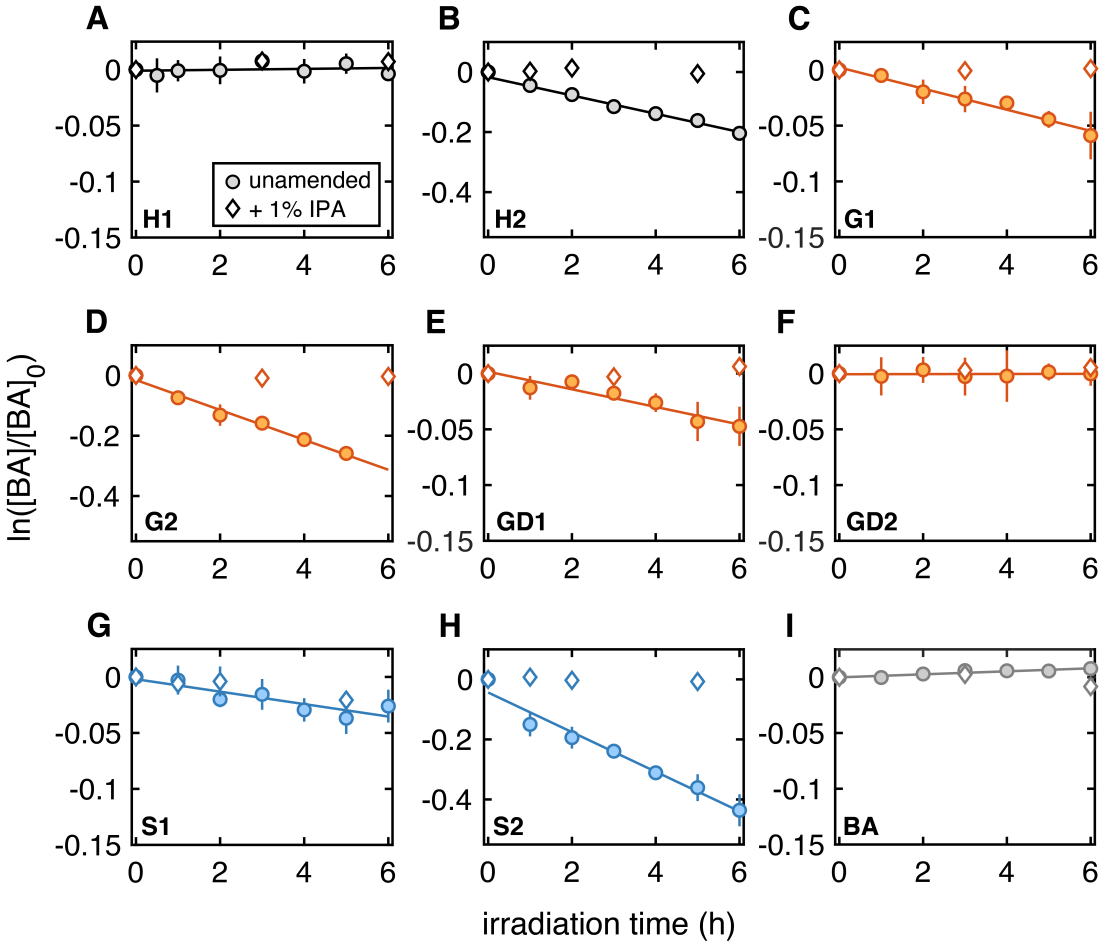

Figure S18: Results of benzoate depletion experiments used to quantify $[OH^{\bullet}]_{ss}$ (filled circles; $[BA]_0 = 10$ μM, $[substrate]_0 = 50$ μM, 6 UV lamps) and to confirm that BA depletion is due to $OH^{\bullet}$ alone (empty diamonds; as before + 1% (v/v) isopropylic alcohol, IPA). Each symbol is the average of at least duplicate experiments and the error bar is the standard deviation or variance. When not visible, the error bar is within the symbol. We used the slopes of the linear regression lines to quantify $[OH^{\bullet}]_{ss}$ according to eq 7 (main text). For **S1** (panel G), the 5 h datapoint was comparable for the two conditions; further tests with, e.g., longer irradiation times or more replicates, should confirm this result. Color code: black, *p*-hydroxyphenyl derivatives; orange, guaiacyl derivatives; blue, syringyl derivatives; grey, benzoate control.

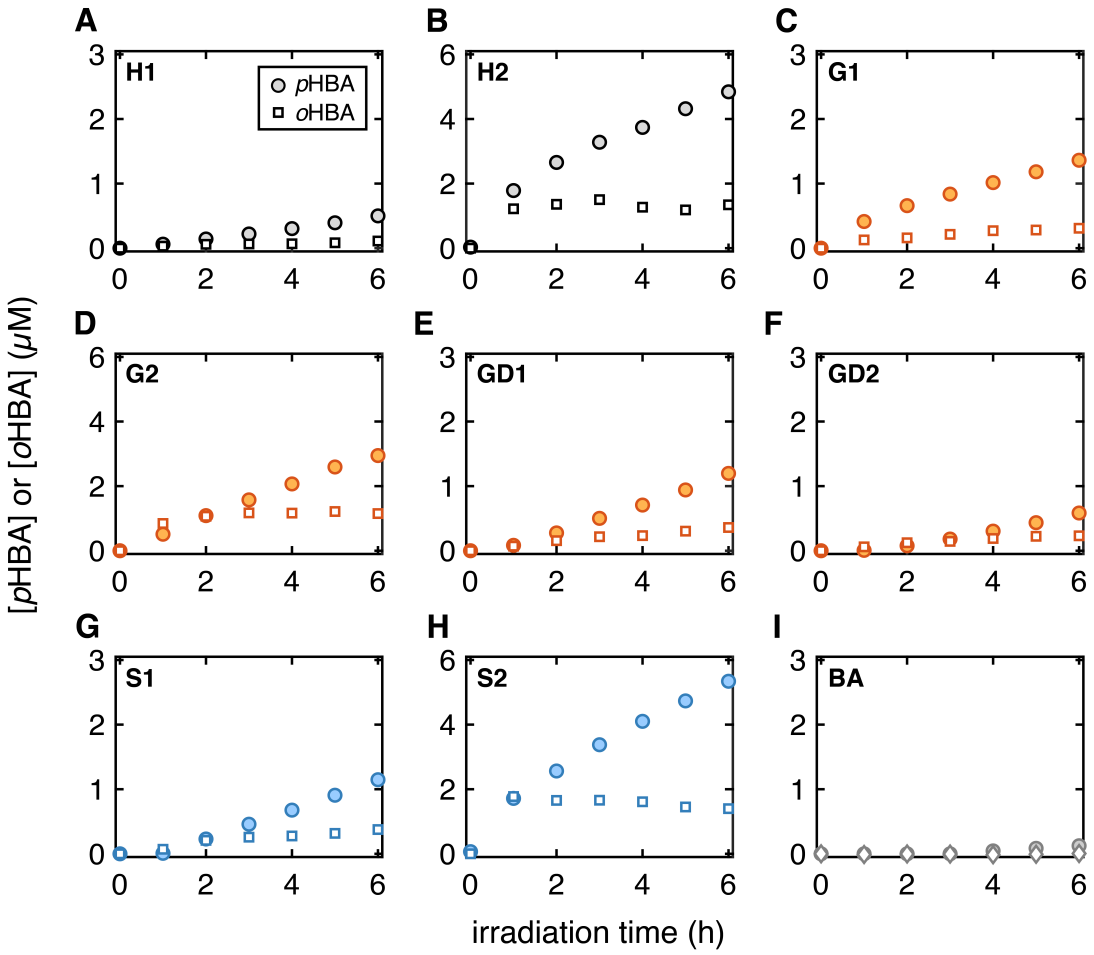

Figure S19: Production of benzoate hydroxyl radical products in experiment employing high probe concentrations ($[BA]_0$ = 1 mM, $[substrate]_0$ = 50 μM, 6 UV lamps). Each symbol is a single experiment; the error is not indicated. The *meta* isomer (*m*HBA) was detected in all cases (but panel I) but is not shown due to difficulties in quantification. Color code: black, *p*-hydroxyphenyl derivatives; orange, guaiacyl derivatives; blue, syringyl derivatives; grey, benzoate control.

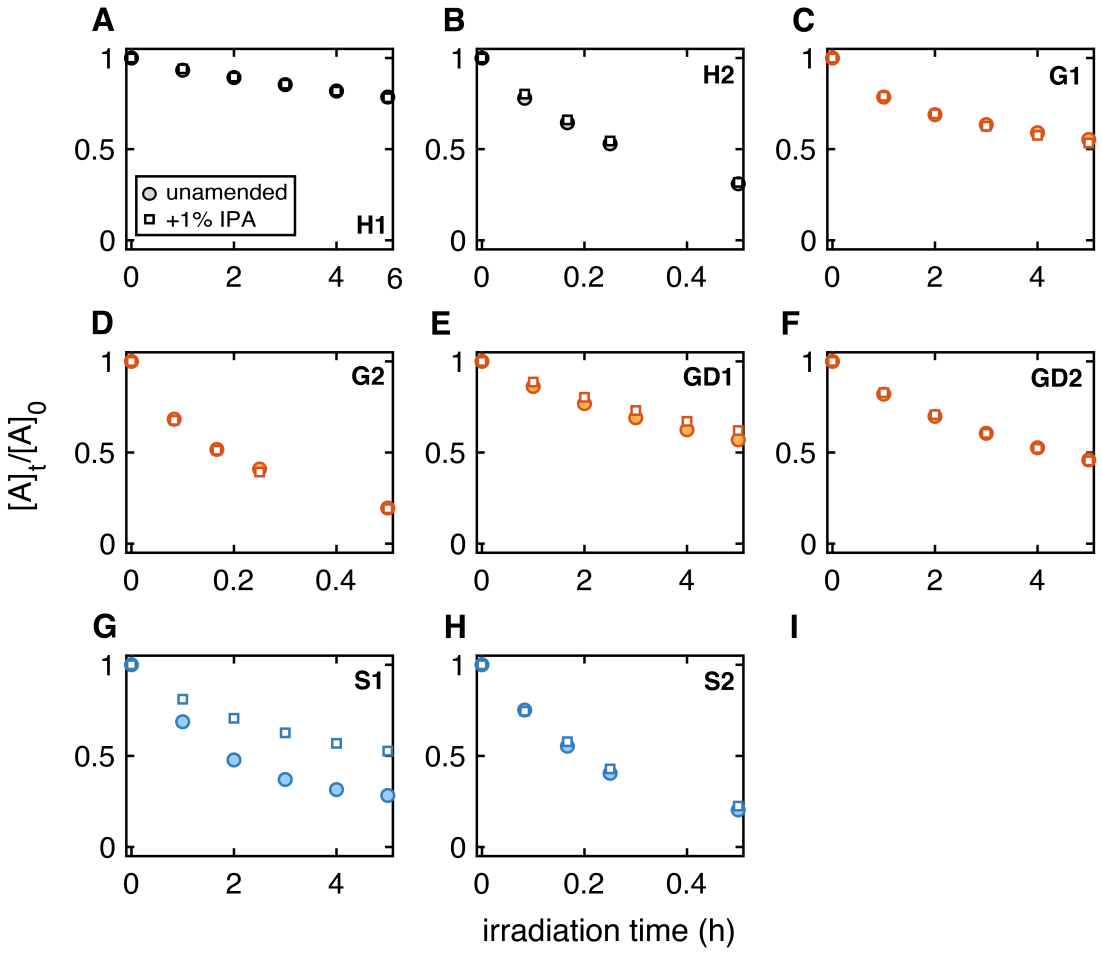

Figure S20: Control experiments showing changes in substrate photodegradation kinetics upon addition of isopropanol (1% IPA, empty squares; $[\text{substrate}]_0 = 50$ μM, 6 UV lamps). These experiment were not performed in duplicate. Note that **S1** depletion kinetics showed $\approx 10-15\%$ variability across repeated experiments, which is considerably higher that what we observed for the other substrates. Therefore, further replicates need to confirm the extent of IPA quenching for this model compound. Color code: black, *p*-hydroxyphenyl derivatives; orange, guaiacyl derivatives; blue, syringyl derivatives.

S10 Estimation of lignin concentrations in DOM

To the authors' knowledge, direct measurements of lignin content in DOM are not available.

Most authors used lignin *biomarkers* as proxies for lignin content. Concentrations of lignin biomarkers are obtained by CuO oxidation followed by GC/MS analyses of the resulting oxidation products and provide a low-end estimate of true lignin concentrations in DOM.[25] Typical concentrations span between 0.24 and 3.12 mg per 100 mg of DOC.[26,27] If we assume a DOM concentration between 5 and 25 $mg_C\ L^{-1}$, realistic for freshwater environments, lignin phenols will be between 12 $\mu g\ L^{-1}$ and 0.78 $mg\ L^{-1}$. These concentrations are at least one order of magnitude lower than we tested in our experiments ($50\ \mu M \approx 6.9 - 14.5$ $mg\ L^{-1}$).

An alternative approach is to use the percent of methoxy aromatic carbon obtained via solid-state ^{13}C NMR. If we assume that -OCH_3 groups are predominantly associated with lignin's guaiacyl and syringyl moieties, this calculation can provide an upper-end estimate of lignin content in DOM. Solid-state ^{13}C NMR showed that $0.7 - 13\%$ of the total signal is attributable to -OCH_3 groups, with most values being around 10%.[28–30] In this case, a $5 - 25\ mg_C\ L^{-1}$ terrestrial DOM sample contains 0.035 to 3.25 $mg_C\ L^{-1}$ of -OCH_3 groups; the range reduces to 0.5 to 2.5 $mg_C\ L^{-1}$ if we use an average methoxy group content of $\approx 10\%$. Unlike lignin phenol biomarkers, this value is well within the range of our solutions, which contain 0.6 $mg_C\ L^{-1}$ (**G** models) or 1.2 $mg_C\ L^{-1}$ (**S** models) of -OCH_3 groups.

References

(1) Wiles, C.; Watts, P.; Haswell, S. J. Clean and selective oxidation of aromatic alcohols using silica-supported Jones' reagent in a pressure-driven flow reactor. *Tetrahedron Letters* **2006**, *47*, 5261–5264.

(2) Ema, T.; Yoshii, M.; Korenaga, T.; Sakai, T. Mechanism-based enzymatic method for reliable determination of absolute configuration of chiral 1-substituted ethanols: combination with NMR method. *Tetrahedron: Asymmetry* **2002**, *13*, 1223–1229.

(3) Fresco, Z. M.; Suez, I.; Backer, S. A.; Fréchet, J. M. J. AFM-Induced Amine Deprotection: Triggering Localized Bond Cleavage by Application of Tip/Substrate Voltage Bias for the Surface Self-Assembly of Nanosized Dendritic Objects. *Journal of the American Chemical Society* **2004**, *126*, 8374–8375.

(4) McNally, A. M. Photochemistry of natural organic matter. Ph.D. thesis, University of Minnesota, 2006.

(5) Noji, M.; Ohno, T.; Fuji, K.; Futaba, N.; Tajima, H.; Ishii, K. Secondary Benzylation Using Benzyl Alcohols Catalyzed by Lanthanoid, Scandium, and Hafnium Triflate. *The Journal of Organic Chemistry* **2007**, *68*, 9340–9347.

(6) Fulmer, G. R.; Miller, A. J. M.; Sherden, N. H.; Gottlieb, H. E.; Nudelman, A.; Stoltz, B. M.; Bercaw, J. E.; Goldberg, K. I. NMR Chemical Shifts of Trace Impurities: Common Laboratory Solvents, Organics, and Gases in Deuterated Solvents Relevant to the Organometallic Chemist. *Organometallics* **2010**, *29*, 2176–2179.

(7) Wimmer, Z.; Saman, D.; Francke, W. Novel Juvenoids of the 2-(4-hydroxybenzyl)cyclohexan-1-one Series. *Helvetica Chimica Acta* **1994**, *77*, 502–508.

(8) Glock, J. et al. Lead-Discovery of bis-Aromatic Alkynes: A Novel Class of Herbicides. *CHIMIA International Journal for Chemistry* **2008**, *62*, 23–28.

(9) Lancefield, C. S.; Westwood, N. J. The synthesis and analysis of advanced lignin model polymers. *Green Chemistry* **2015**, *17*, 4980–4990.

(10) Reddy, M. V. R.; Mallireddigari, M. R.; Cosenza, S. C.; Pallela, V. R.; Iqbal, N. M.; Robell, K. A.; Kang, A. D.; Reddy, E. P. Design, Synthesis, and Biological Evaluation of

(*E*)-Styrylbenzylsulfones as Novel Anticancer Agents. *Journal of Medicinal Chemistry* **2008**, *51*, 86–100.

(11) Yeom, C.-E.; Kim, H. W.; Lee, S. Y.; Kim, B. M. DBU-Mediated Mild and Chemoselective Deprotection of Aryl Silyl Ethers and Tandem Biaryl Ether Formation. *Synlett* **2007**, *1*, 0146–0150.

(12) Martinez, C. H. R.; Dardonville, C. Rapid Determination of Ionization Constants (pK_a) by UV Spectroscopy Using 96-Well Microtiter Plates. *ACS Medicinal Chemistry Letters* **2013**, *4*, 142–145.

(13) Bunting, J. W.; Stefanidis, D. A systematic entropy relationship for the general-base catalysis of the deprotonation of a carbon acid. A quantitative probe of transition-state solvation. *Journal of the American Chemical Society* **1990**, *112*, 779–786.

(14) Vandenbelt, J. M.; Henrich, C.; Vanden Berg, S. G. Comparison of pK_a Values Determined by Electrometric Titration and Ultraviolet Absorption Methods. *Analytical Chemistry* **1954**, *26*, 726–727.

(15) Bordwell, F. G.; Cooper, G. D. Conjugative Effects of Methylsulfonyl and Methylthio Groupings. *Journal of the American Chemical Society* **1952**, *74*, 1058–1060.

(16) Luchtefeld, R.; Luo, R.; Stine, K.; Alt, M. L.; Chernovitz, P. A.; Smith, R. E. Dose Formulation and Analysis of Diapocynin. *Journal of Agricultural and Food Chemistry* **2008**, *56*, 301–306.

(17) Fisher, J. H.; Hawkins, W. L.; Hibbert, H. Studies on Lignin and Related Compounds. LIV. Synthesis and Properties of Glycosides Related to Lignin. *Journal of the American Chemical Society* **1941**, *63*, 3031–3035.

(18) Borduas-Dedekind, N.; Ossola, R.; David, R. O.; Boynton, L. S.; Weichlinger, V.; Kanji, Z. A.; McNeill, K. Photomineralization mechanism changes the ability of dissolved organic matter to activate cloud droplets and to nucleate ice crystals. *Atmospheric Chemistry and Physics* **2019**, *19*, 12397–12412.

(19) Ossola, R.; Tolu, J.; Clerc, B.; Erickson, P. R.; Winkel, L. H. E.; McNeill, K. Photochemical Production of Sulfate and Methanesulfonic Acid from Dissolved Organic Sulfur. *Environmental Science & Technology* **2019**, *19*, 507–516.

(20) Meyet, J.; Searles, K.; Newton, M. A.; Wörle, M.; van Bavel, A. P.; Horton, A. D.; van Bokhoven, J. A.; Copéret, C. Monomeric Copper(II) Sites Supported on Alumina Selectively Convert Methane to Methanol. *Angewandte Chemie International Edition* **2019**, *58*, 9841–9845.

(21) Buxton, G. V.; Greenstock, C. L.; Helman, W. P.; Ross, A. B. Critical Review of rate constants for reactions of hydrated electrons, hydrogen atoms and hydroxyl radicals in Aqueous Solution. *Journal of Physical and Chemical Reference Data* **1988**, *17*, 513–886.

(22) Fry, V. A.; Istok, J. D.; Semprini, L.; O'Reilly, K. T.; Buscheck, T. E. Retardation of Dissolved Oxygen Due to a Trapped Gas Phase in Porous Media. *Ground Water* **1995**, *33*, 391–398.

(23) Ossola, R.; Clerc, B.; McNeill, K. Mechanistic Insights into Dissolved Organic Sulfur Photomineralization through the Study of Cysteine Sulfinic Acid. *Environmental Science & Technology* **2020**, *54*, 13066–13076.

(24) Schymanski, E. L.; Jeon, J.; Gulde, R.; Fenner, K.; Ruff, M.; Singer, H. P.; Hollender, J. Identifying Small Molecules via High Resolution Mass Spectrometry: Communicating Confidence. *Environmental Science & Technology* **2014**, *48*, 2097–2098.

(25) Cooper, W. T.; Chanton, J. C.; D'Andrilli, J.; Hodgkins, S. B.; Podgorski, D. C.; Stenson, A. C.; Tfaily, M. M.; Wilson, R. M. A History of Molecular Level Analysis of Natural Organic Matter by Fticr Mass Spectrometry and The Paradigm Shift in Organic Geochemistry. *Mass Spectrometry Reviews* **2022**, *41*, 215 – 219.

(26) Reuter, H.; Gensel, J.; Elvert, M.; Zak, D. Direct Analysis of Lignin Phenols in Freshwater Dissolved Organic Matter. *Analytical Chemistry* **2017**, *89*, 13449–13457.

(27) Meyers-Schulte, K. J.; Hedges, J. I. Molecular evidence for a terrestrial component of organic matter dissolved in ocean water. *Nature* **1986**, *321*, 61–63.

(28) Mao, J.; Kong, X.; Schmidt-Rohr, K.; Pignatello, J. J.; Perdue, E. M. Advanced Solid-State NMR Characterization of Marine Dissolved Organic Matter Isolated Using the Coupled Reverse Osmosis/Electrodialysis Method. *Environmental Science & Technology* **2012**, *46*, 5806–5814.

(29) Zhou, Z.; Hua, B.; Cao, X.; Yang, J.; Olk, D. C.; Deng, B.; Liu, F.; Li, R.; Mao, J. Chemical composition of dissolved organic matter from various sources as characterized by solid-state NMR. *Aquatic Sciences* **2015**, *77*, 595–607.

(30) Zigah, P. K.; Minor, E. C.; Abdulla, H. A. N.; Werne, J. P.; Hatcher, P. G. An investigation of size-fractionated organic matter from Lake Superior and a tributary stream using radiocarbon, stable isotopes and NMR. *Geochimica et Cosmochimica Acta* **2014**, *127*, 264–284.